Chapter 4

1st Part: Flexible Transparent Conductors with a percolated Ag nanostructure and its Application as Efficient Self-bias Plasmonic Photodetector

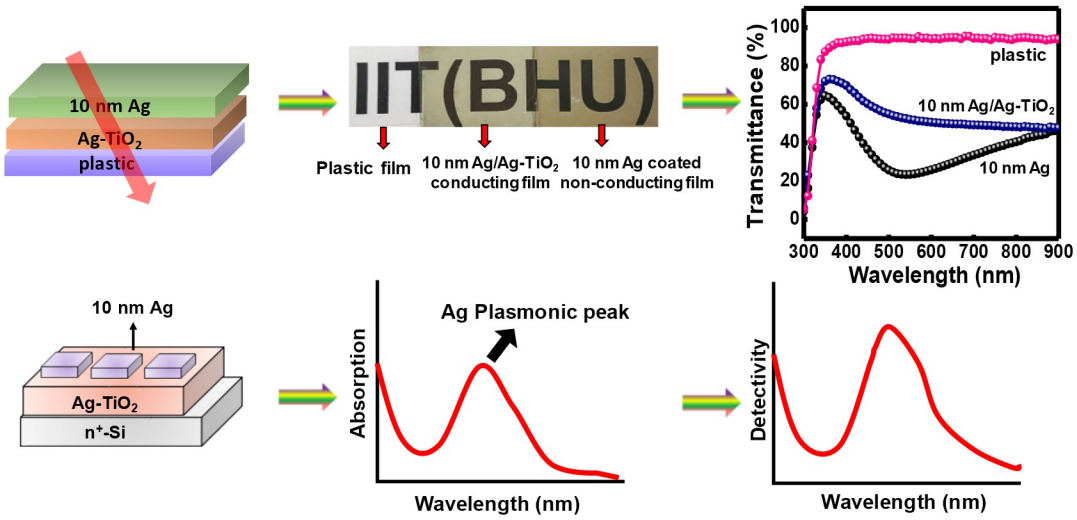

Chapter 4

This chapter mainly focuses on development of a percolated silver (Ag) nanostructured-based transparent conductor and used it for the applications of self-bias plasmonic photodetector. Device has been deposited by physical vapor deposition (PVD) technique where lateral growth of Ag has been enhanced by a pre-deposited Ag-TiO_2 thin film. This Ag-TiO_2 film has embedded Ag nanoparticles (NPs) within TiO_2 thin film which is grown in a low temperature (100°C) solution processed technique that includes LTO thin film deposition by a sol-gel method followed by ion-exchange ($Li^+ \rightarrow Ag^+$) process to yield an Ag-TiO_2 thin film. The percolated Ag network has appeared as soon film mass-thickness reaches close to 10 nm, resulting in an abrupt drop of electrical resistivity of the film. This percolated Ag nanostructured thin film (10 nm Ag/Ag-TiO_2/plastic) has resistivity of ~ 50 ohm/□ and an average visual transmittance of >70% up to 450 nm. In higher wavelength range, transparency gradually reduces, and it reaches to ~50% at 600 nm which is mostly due to the plasmon absorption of this film. By utilizing its combined optical transparency and surface plasmon absorption, this film has been used to develop plasmonic hot electron photodetectors where Ag-thin film works as transparent electrode as well as plasmon induced photo-excited hot electron generation. Device has been fabricated on a highly doped n type Si (n^+-Si) with a metal-semiconductor-metal (M-S-M) device geometry. External quantum efficiency (EQE) data reveal that photocurrent of this device is mostly generated in the plasmonic absorption region with a peak detectivity of 2.84×10^{12} Jones at 510 nm under -3V external bias. Besides, the device shows fast response with a response time of ~25 ms.

4.1 Introduction

Until now, indium tin oxide (ITO) has mostly used as a transparent conductor (TC) that can achieve transparency (>90%) with quite excellent electrical conductivity.[116, 117] However, these ITO-based transparent electrodes (TEs) are quite expensive due to the use

of indium, which is one least abundant mineral on earth.[119] Besides, due to the inorganic nature of ITO, it has poor mechanical flexibility.[118] Relatively, carbon-based TC like carbon nanotube[175] and graphene[176] has higher mechanical flexibility with excellent optical transparency. Although, the electrical conductivity of these ITO or carbon based TCs are quite lower with respect to metals like Ag, Au, and Cu.[120] In contrast, metals have significant refractive index (n) that limit the development of metal based TEs. Among different metals, Ag has the least n (~0.05) in the visible range of light and has been widely studied for TC development.[177-179] Most of those studies are either Ag nanowire[121, 180, 181] based or oxide/Ag/oxide multi-stack thin film[122, 182] based where ~10 nm Ag film is commonly used. These Ag-based TCs have higher electrical conductivity than ITO with acceptable mechanical flexibility which could be an ideal TC electrode for flexible electronics.[123, 183] However, Ag nanostructured or Ag thin films have very strong plasmonic absorption which is a key barrier to achieve high optical transparency of those films.[124, 184] Besides, due to higher reactivity of Ag nanostructure, long term stability of these Ag-based TCs are not as good as ITO.[123, 185]

Although plasmonic absorption is a key bottleneck of developing metal based highly transparent conductors, it's useful for developing various optoelectronics devices including solar cell, plasmonic photodetector, memory device, sensors, and light emitting diodes.[186-189] A number of group claims that the plasmonic effect of electrode can add hot-electron induced photocurrent which can be beneficial for photocurrent generation of solar cell, photodetector and photo-electrochemical H_2 generation.[140, 190, 191] When electromagnetic waves (EMW) interact with a metal MNPs, part of that EMW is scattered and the rest of the part is absorbed by MNPs due to the SPR. This SPR absorption of MNPs increase whereas scattering reduces with reducing particle size. Besides, shape of MNPs, the relation of dielectric constant of MNPs and surrounding are also important parameters for SPR related absorption of MNPs.[81] Due to the SPR, MNPs either generate electron-hole pairs or go through radiative decay to the far field. Again, this generated electron-hole pair can produce hot-electron through non-thermal electron distribution via electron-electron scattering.[55, 192] To utilize this hot-electron for optoelectronics device application, a semiconductor-metal Schottky junction is required through which it can be injected to the semiconductor within a very short period of time (<100 fs), before non-

radiative energy relaxation of hot-electron through electron-phonon scattering. Besides, for efficient electron injection of this hot-electron in the Schottky junction, a low barrier height (Φ_b) Schottky junction is required.[193, 194] In plasmonic devices, this metal-semiconductor Schottky junction have been developed by varsities ways like; by depositing metal thin film on a nanostructured semiconductor surface followed by inert atmosphere annealing to form MNPs,[195] MNPs-metal oxide thin film,[196, 197] semiconductor-metal thin film heterojunction etc.[198, 199] In addition, several reports claims that the optoelectronics devices performance can be improved by using a plasmonic electrodes.[169] In a plasmonic photodetector, the contribution of hot electron is commonly realized from the EQE measurement that indicated a strong photocurrent generation in the plasmonic absorption region of MNPs. However, there are very limited reports that demonstrated the similarity of plasmonic absorption and EQE spectra of the device. Moreover, EQE values of those devices are also quite poor.

This section of the chapter has described a low cost deposition technique of Ag based TC film. For this, 10 nm Ag has been deposited on top of an Ag-TiO_2 thin film at low temperature (~100°C) to fabricate TC films, enables us to deposit this conducting film on a plastic substrate. The growth of Ag NPs inside TiO_2 matrix, helps in controlling the size and uniform distribution of Ag NPs throughout the plastic substrate. At the initial stage of Ag growth, it has been observed that the nucleation density of Ag NPs on this TC film is much higher than bare plastic substrate. However, after a critical size growth of those grains, granular film undergoes a solid-state dewetting process which makes it possible to deposit percolated finger-like Ag nanostructured thin film. The presence of metal-oxide TiO_2 layer offer structural support to ensure long-term stability and durability of this TC film. So, the combination of TiO_2 and Ag NPs leverages the strengths of both materials. As a consequence, the resistivity of the film dropped suddenly while optical transparency has been maintained ~70% in the violet-blue region. However, it drops to ~50-60% in the higher wavelength region of light due to the plasmonic absorption of the film. To analyze the surface phenomena of this percolated finger-like Ag nanostructured, we developed a percolation model which tells about the nature of percolation threshold during growth. Besides, this transparent-conducting Ag film has been used as a plasmonic electrode for developing high performance hot-electron photodetectors. Device has been fabricated on a

n^+-Si substrate that shows extremely high detectivity with fast response speed. The UV-Vis absorption spectra of Ag based TC film shows a strong SPR absorption, has an excellent spectral matching with the EQE spectra of the photodetector, implying the major contribution of hot-electron in the photocurrent generation of the device.

4.2 Experimental Section

4.2.1 Synthesis of Materials

The synthesis process for $Li_4Ti_5O_{12}$ via low temperature solution process technique has been explained in **Chapter 2 Chapter 2 Section 2.1.1.** PMMA is used as a protective coating for TC film. The solution is prepared by standard method, reported in **Chapter 2 Section 2.1.7**.

4.2.2 Fabrication of TC Film

The Ag/Ag-TiO_2 based TC film has been fabricated on a flexible PET substrate and the fabrication steps has been explained **Chapter 2 Section 2.3.2**, and schematically present in **Figure 2.7**. For fabrication of a photodetector, these optimized 10 nm Ag/Ag-TiO_2 TC thin film have been used as transparent electrode to develop plasmonic photodetectors in a photodiode geometry which is schematically present in **Figure 2.8**.

4.3 Result and discussion

4.3.1 XRD Analysis of Thin Films

For the crystal phase identification of thin films, we prepared XRD samples on a plastic substrate. **Figure 4.1** shows the XRD patterns of LTO, Ag-TiO_2, 10 nm Ag/Ag-TiO_2, and 10 nm Ag thin film on bare plastic substrate. In the thin-film XRD pattern of LTO, two intense peaks at 2θ ~35.55º and 43.3º have been observed which come from the reflection planes of (311) and (400) respectively (JCPDS file no. 490207). The XRD pattern of Ag-TiO_2 thin film shows three intense peaks at 2θ ~ 25.1º, 37.72º and 43.7º which corresponds to anatase TiO_2 (101), Ag (111) and Ag (200) respectively. These intense broad peaks of Ag NPs are confirming the formation of Ag NPs inside TiO_2 matrix after ion-exchange process. The prepared TC film (10 nm Ag/Ag-TiO_2) shows similar peak positions with much higher intensity at 2θ ~25.1º, 37.72º, and 43.7º corresponding to TiO_2 (101), Ag (111), and Ag

(200) respectively. As a reference, we did an XRD analysis of 10 nm Ag film on a bare plastic substrate, which shows peak positions at 2θ ~ 37.72º and 43.7º corresponding to Ag (111) and Ag (200) respectively (JCPDS file no 897322).

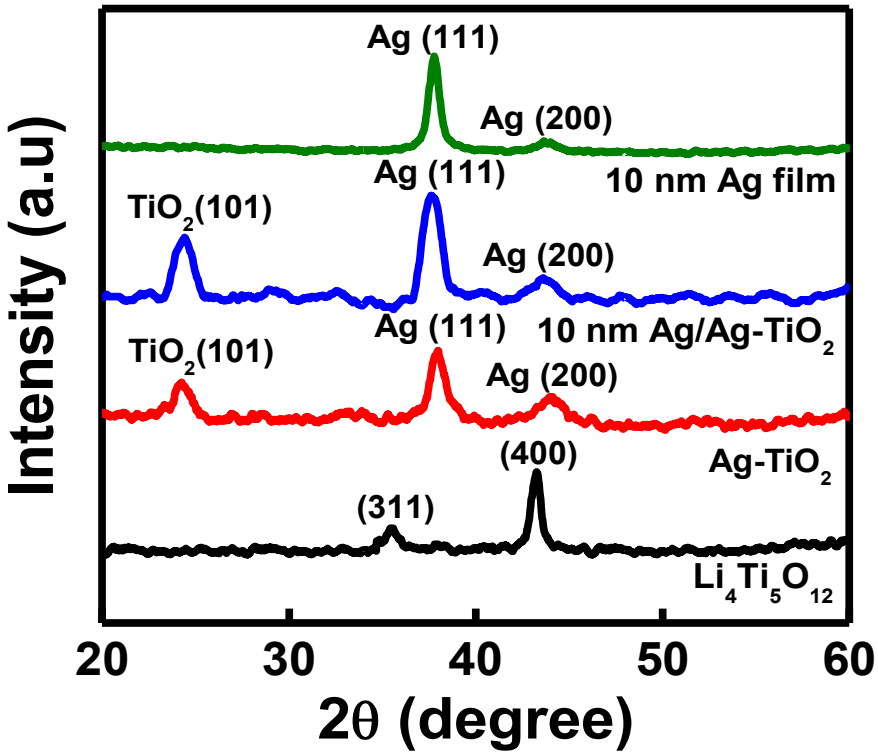

Figure 4.1 XRD pattern of step-by-step growth of TC film deposited on plastic substrates.

4.3.2 Electrical and optical characterization of TC Film

To measure the electrical resistivity of as prepared TC films, parallel Ag electrodes (thickness ~50 nm) of separation 0.45 mm have been deposited over the film. **Figure 4.2a)** depicts the semi-log plot of current density vs voltage (J-V) graphs of Ag/Ag-TiO_2 thin films with different Ag film thickness varying from 10 nm to 14 nm. This data implies that conductivity of 14 nm Ag/Ag-TiO_2 film is ~ one order higher w.r.t the 10 nm Ag film/Ag-TiO_2 film. Besides, it is observed that a large amount of current is achievable by applying a relatively modest voltage of 0.05 V. Besides, to test the film flexibility, we have examined the conductivity test with different bending cycles of (10 nm Ag/Ag-TiO_2) thin film which is shown **Figure 4.2b)**. This study indicates that conductivity of the film remains almost unaltered even after 100 cycles of bending with a fixed value of bending radius 4 mm, suggesting that film is highly durable for the fabrication of high performance flexible opto-

electronic devices. We have also coated a very thin layer of PMMA polymer as a protective layer on the top of the film to enhance the durability from humidity, oxidation, and abrasion. Following PMMA coating, an experiment is conducted to visualize the influence of the film's performance. After coating, films electrical conductivity and optical transparency (PMMA/10 nm Ag/Ag-TiO_2/plastic) data shows almost similar performance compared to uncoated PMMA film (**Figure 4.2c**). Besides, resistance vs temperature of (10 nm Ag/Ag-TiO_2) samples has been measured by four probe methods. The sample shows moderate drop in resistance up to 200 K which indicates fully metallic behavior of the TC film (**Figure 4.2d**).

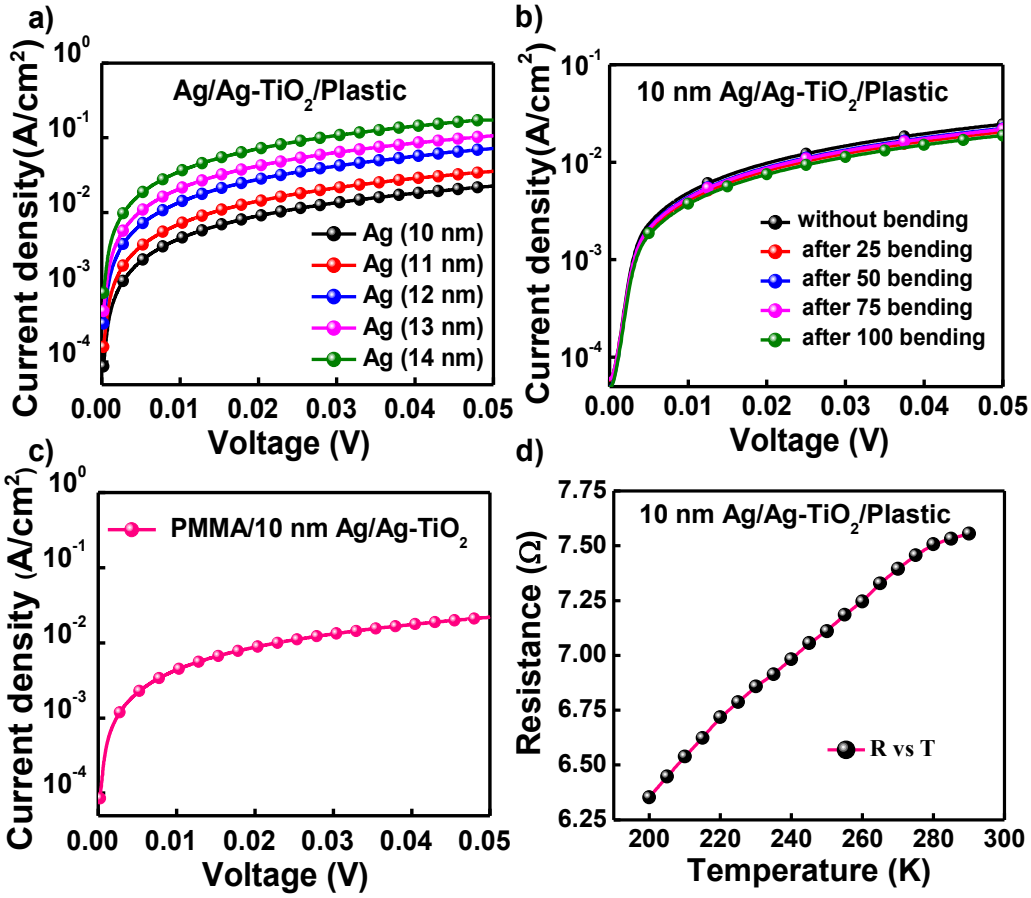

Figure 4.2a) Semi-log graph of electrical current density vs voltage of Ag/Ag-TiO_2 based TC film with Ag film thickness varying from 10 nm to 14 nm **b)** exhibits mechanical stability up to 100 bending cycles **c)** performance of TC film with PMMA as a protecting layer and **d)** variation of resistance and temperature under four probe measurement upto 200 K.

The optical transmittance of Ag/Ag-TiO_2 film for different Ag film thickness has been investigated, depicted in **Figure 4.3a)**. This data implies that 10 nm conducting film has an excellent optical transparency of 73-70 % in the blue region of 380 - 400 nm which is reduced to ~ 50 % for longer wavelengths of light. The reduction of transparency at higher wavelength is mainly due to the plasmonic absorption of Ag/Ag-TiO_2 thin film. With PMMA coat, film shows almost same transparency as compared to original TC film (**Figure 4.3b)**). The phenomena of conductivity and transparency are interconnected, leading to a trade-off. The precise form of this dependency is defined by the impact of varying deposition conditions on the electro-optical characteristics of these layers. However, under ideal circumstances, both sheet resistance (R_{sh}) and transparency (T) are greatly affected by the film thickness. **Table 4.1** shows the combined electrical and optical data of these prepared TC films. **Figure 4.3c)** represents the variance of sheet resistance and visible transmittance with the film thickness. Therefore, it can be concluded that the electrical conductivity of the film increases with increasing Ag thickness, but also it reduces the optical transparency (**Figure 4.3c)**).

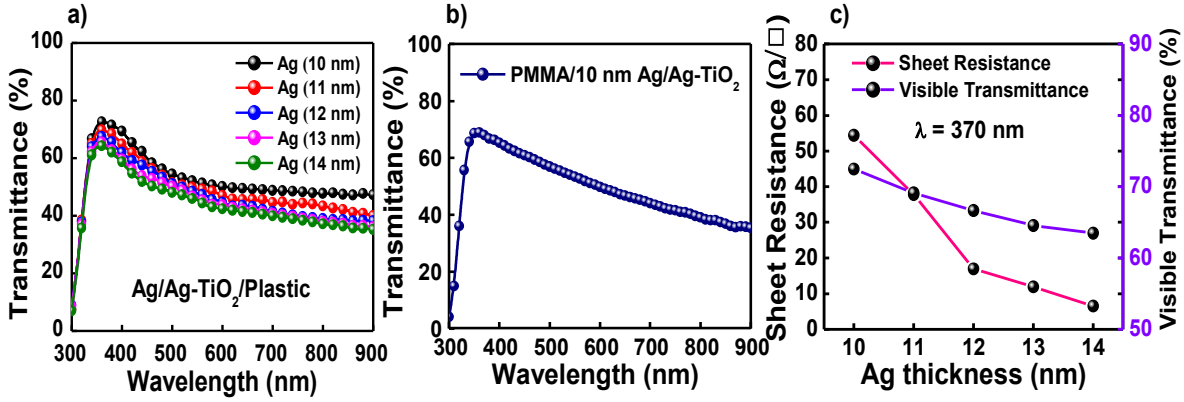

Figure 4.3a) Optical transparency of TC film with different Ag film thickness **b**) optical transparency of TC film with PMMA protecting layer, and **c)** variation of sheet resistance and visible transmittance under different Ag film thickness.

Table 4.1 Electrical Sheet Resistance and Visible Transmittance data of (Ag/Ag-TiO_2) based transparent conducting films by altering the thickness of Ag film.

The thickness of Ag film (nm)	Sheet Resistance (Ω/□)	Visible Transmittance (%) λ= 370 nm	Visible Transmittanc (%) λ= 500 nm
10	54.36	72.46 %	54.49 %
11	37.79	69.11 %	51.47 %
12	16.93	66.64 %	51.15 %
13	11.91	64.56 %	50.28 %
14	6.51	63.48 %	48.12 %

4.3.3 Surface Morphology (HR-SEM, AFM & HR-TEM) Study

HR-SEM is performed to look at the surface morphological structure of Ag/Ag-TiO_2 thin film. During Ag film deposition, morphological changes of film surface have been depicted in **Figure 4.4**. It has been observed when 10 nm Ag is deposited on top of Ag-TiO_2 film by thermal evaporation, individual Ag islands are percolated to interconnected finger-like structure (**Figure 4.4c)**),whereas demonstrate the earlier development stages of the film which consist of individual compact islands separated by nano-gaps (**Figure 4.4a&b)**). Because of these morphological changes, suddenly conductivity of the 10 nm Ag film increases by several order and transparency of the film also increases. This sudden variation of surface morphology originated from the swiftly merge of separated islands into a bigger one which are finally interconnected. Again, this morphology is not a fully coalesced structure, rather it is creating percolation structure with minimal wiping.[200] As long as film thickness reaches to 10 nm, the effective coverage area for this percolated film becomes quite high (~70%). This is because the empty channels between the elongated structures are quite thin in comparison to the width of the structures. With further deposition of Ag, those channels are mostly filled as shown in **Figure 4.4d)**, resulting in a complete continuous film.

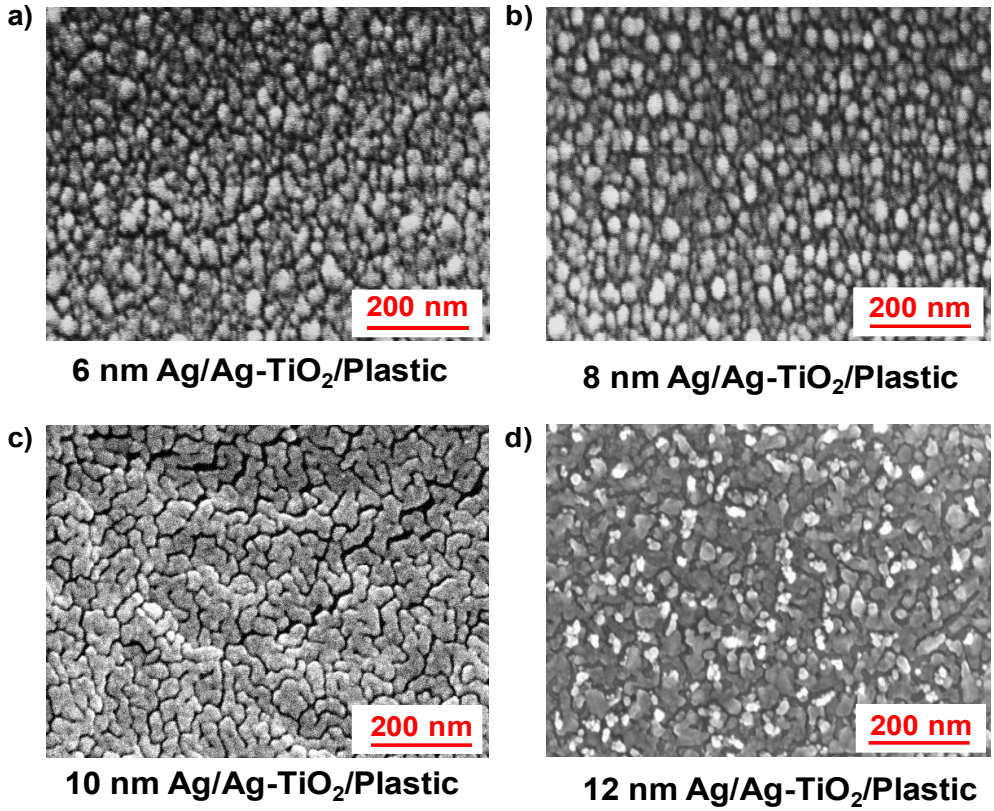

Figure 4.4 FE-SEM photographs of Ag/Ag-TiO_2 thin film at room temperature. Each photograph's average film thickness is listed below. **a&b)** early stage of growth and coalescence of islands **c)** percolating structures **d)** overgrowth percolated structures.

Moreover, TiO_2 metal-oxide also play an important role to reach this percolation threshold at very low thickness of Ag deposition. TiO_2 has a high surface energy, which help Ag NPs nucleate more easily. When Ag is deposited onto the TiO_2 surface, the high surface energy sites on TiO_2 act as nucleation centers, promoting the initial formation of Ag NPs. Besides, TiO_2 stabilize tiny Ag NPs by preventing their agglomeration, leading to a more uniform distribution, which promote better electrical conductivity & visual transparency of the film. For comparison, a set of reference Ag thin films of different mass-thickness (6, 8, 10 and 12 nm) have been grown on bare plastic substrates. The HR-SEM pictures of those films (**Figure 4.5a,b,c&d)**) show that all films are composed of individual isolated islands and doesn't show any conductivity variation up to 14 nm of mass-thickness deposition of Ag, which implies the key role of underlying Ag-TiO_2 thin film for percolated Ag growth.

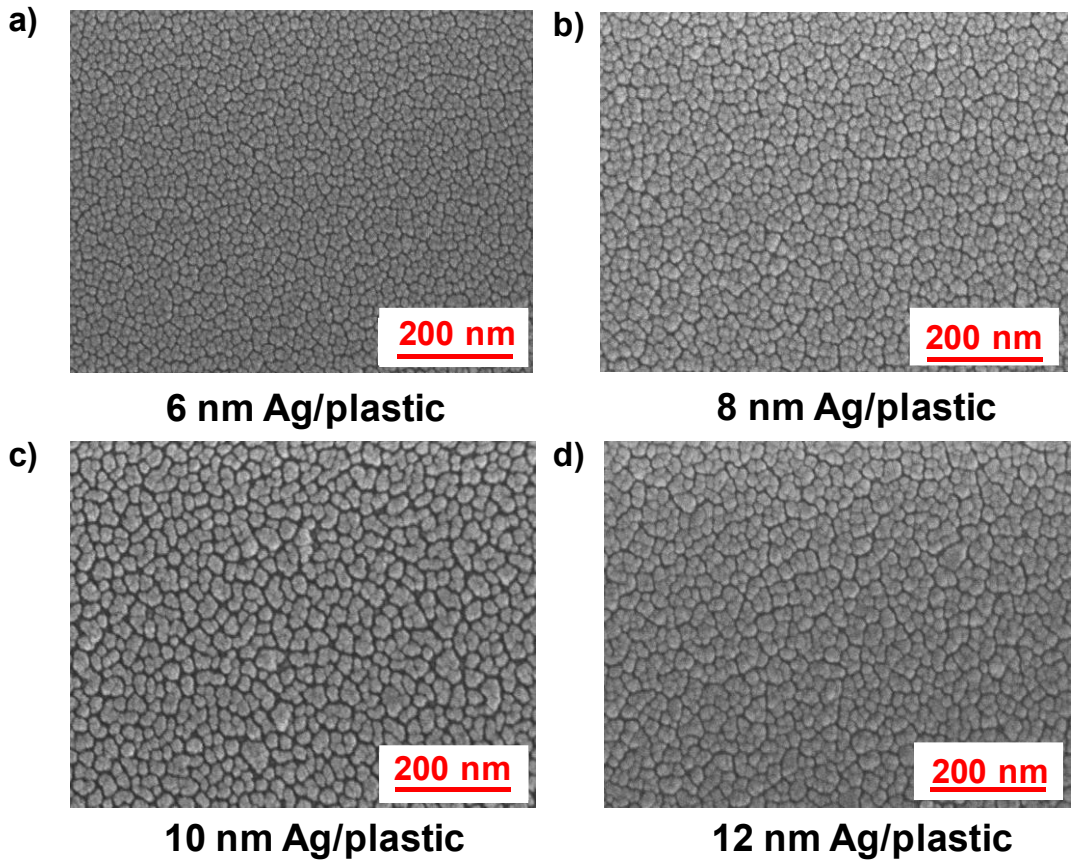

Figure 4.5 SEM images of evaporated Ag on bare plastic at ambient temperature. The surface morphology of Ag film of mass thickness **a)** 6 nm **b)** 8 nm **c)** 10 nm and **d)** 12 nm, which shows the compact separate Ag islands.

An energy- dispersive X-ray spectrometer (EDX) attached to the HR-SEM instrument is used to figure out the contents and amount of metallic elements in 10 nm Ag/Ag-TiO_2 sample is shown in **Figure 4.6a&b)**, which confirms the presence of Ag, Ti, and O uniformly throughout the film. Moreover, the cross-sectional SEM image Ag/Ag-TiO_2 film is shown in **Figure 4.6c)** and obtained thickness of the Ag film is ~ 10 nm and Ag-TiO_2 is ~ 20 nm. The thickness of the Ag film is similar to the recorded thickness obtained from the DTM thickness monitor (~10 nm) of the PVD unit.

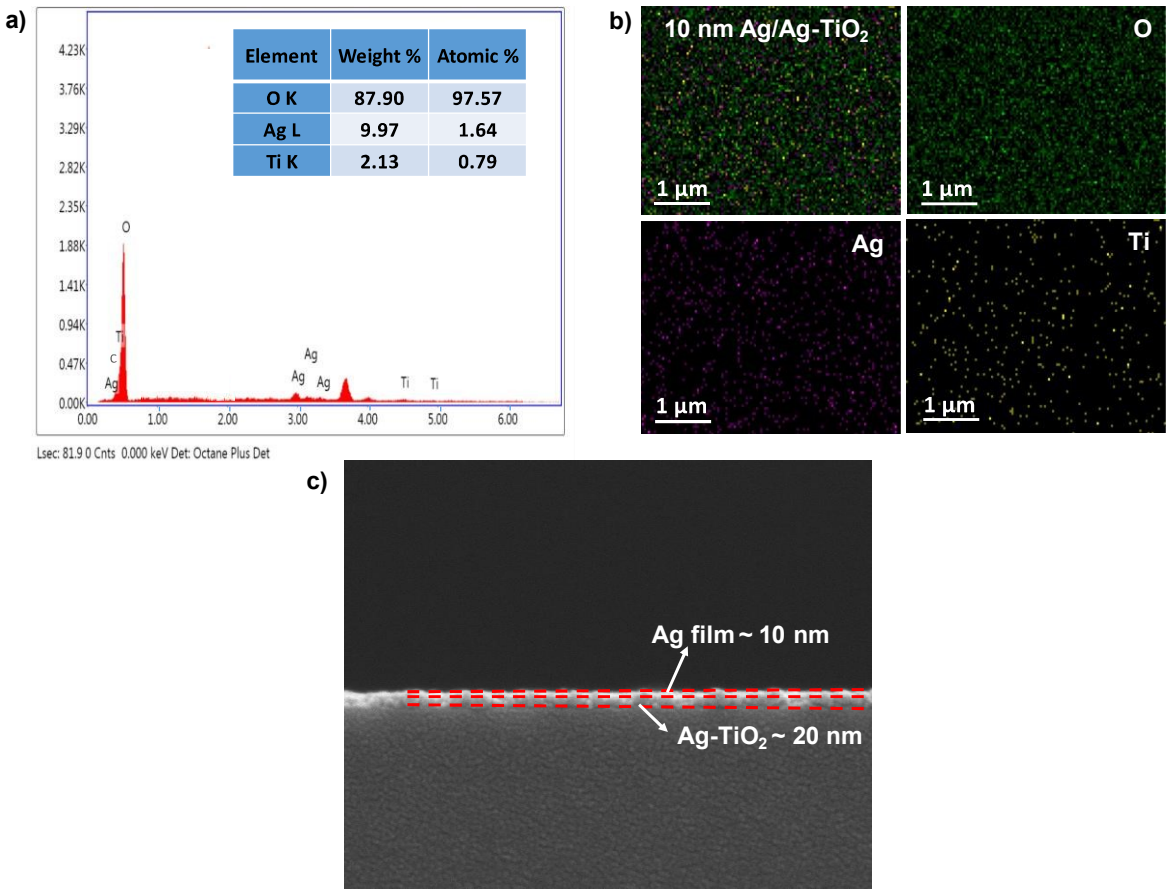

Figure 4.6a) Energy dispersive spectra of 10 nm Ag/Ag-TiO_2/plastic thin film, with the elemental composition determined by EDS displayed in the inset **b)** EDS mapping of (i) 10 nm Ag/Ag-TiO_2 thin film (ii) O, (iii) Ag and (iv) Ti **c)** cross-section SEM image of TC film to determine the thickness of the each individual layer.

AFM is used to describe the surface morphology in more detail, specifically to recognize the surface roughness (R_{rms}). An unconventional surface roughness is observed with increasing Ag film thickness on plastic substrates. It is found that in the lower thickness of Ag film (6 nm Ag/Ag-TiO_2), surface r.m.s roughness ~ 3.6 nm is quite high. However, it decreases to ~ 2.8 nm as soon mass-thickness reaches to 8 nm. Most interestingly, the film roughness reduces to ~ 1.75 nm as soon as mass-thickness of Ag reaches to 10 nm which becomes possible due to the flat finger-like percolated network formation as shown in **Figure 4.7a&b)**.

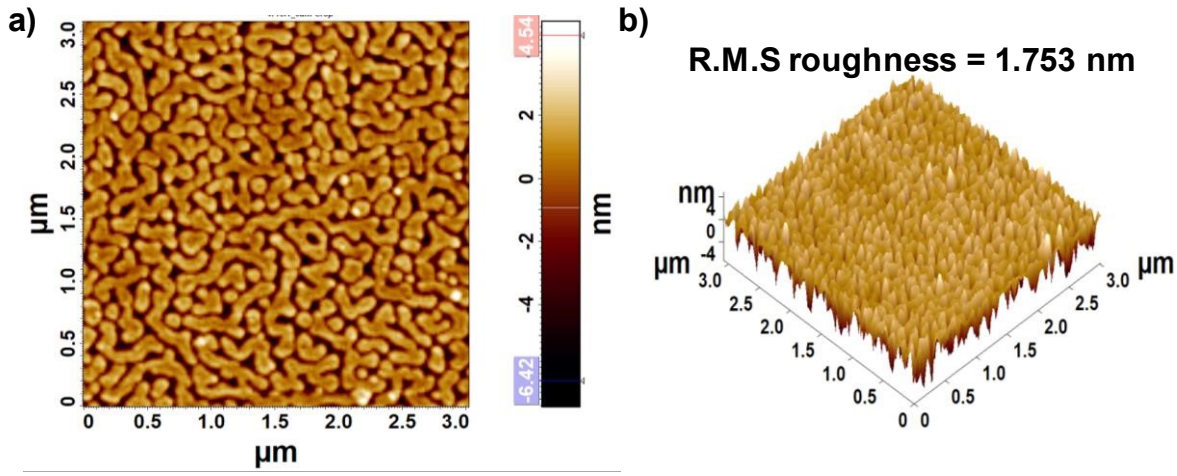

Figure 4.7a) 2-D and **b)** 3-D AFM image of 10 nm Ag/Ag-TiO_2 film ($R_{r.ms}$ ~ 1.75 nm) on plastic PET substrate.

Although, this roughness increases gradually if further growth of Ag film is continued. Besides, the reference 10 nm Ag on plastic substrate also shows high roughness of around ~ 5.2 nm. Surface morphology and their roughness value for different Ag thickness ((6,8,12 nm Ag/Ag-TiO_2) samples and reference (Ag 10 nm/plastic) sample is shown in supplementary data in (**Figure 4.8a,b,c&d)**) and **Table 4.2** . From this study, it is clear that Ag is initially forming individual isolated islands or clusters that have larger vertical growth, resulting in its higher roughness. However, after 8 nm mass-thickness of Ag deposition, lateral growth dominates and finally an abrupt change of surface morphology is evolved as soon this thickness reaches to 10 nm that reduces the surface roughness significantly. This phenomenon is comparable to the thin film dewetting of thin film which normally required higher temperature to evolve such structure.[201, 202] Although in this study, it appears during room temperature Ag growth during physical vapor deposition when grain size of Ag crosses a critical size.

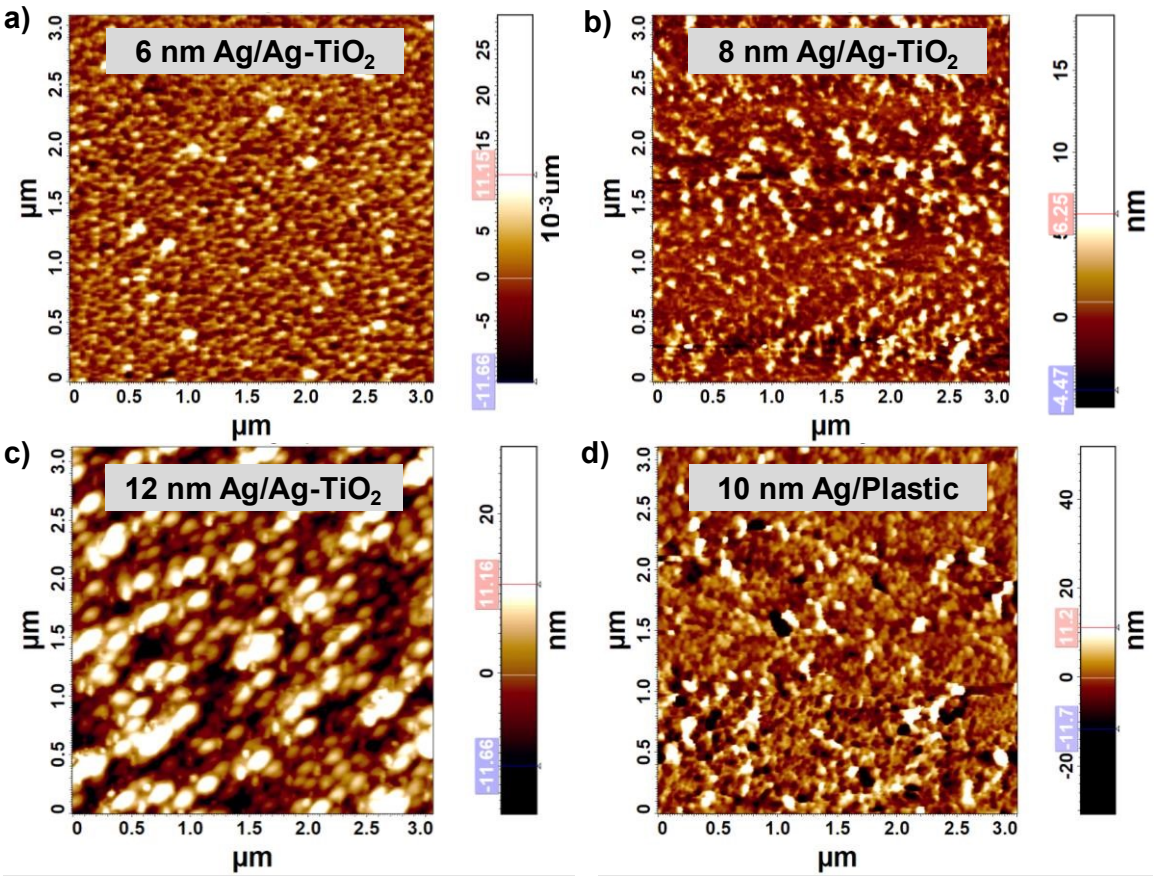

Figure 4.8 2D AFM image of prepared Ag film on Ag-TiO_2 thin film with thickness of **a)** 6 nm **b)** 8 nm and **c)** 12 nm. **d)** AFM image of 10 nm Ag on bare plastic.

Table 4.2 R.M.S Roughness Value for Different Mass Thickness of Ag film

Ag Film	R.M.S Roughness
6 nm Ag/Ag-TiO2/Plastic	3.59
8 nm Ag/Ag-TiO2/Plastic	2.83
10 nm Ag/Ag-TiO2/Plastic	1.75
12 nm Ag/Ag-TiO2/Plastic	6.93
10 nm Ag/Plastic	5.23

The Newman-Ziff cluster algorithm which is a theoretical simulation model based on 2-D square lattice has been used to understand the nature of growth around percolation.

According to their model, when the percolation threshold (P_C) reaches ~ 0.6, percolation starts.[203] The SEM image of 10 nm Ag/Ag-TiO_2 film has been taken as input of this algorithm where the effective coverage area for this percolated film has been considered as P_C (~ 0.7) that determined by ImageJ software. Outcome of this simulation has given the variation of mean cluster size (S) with percolation (P), percolation probability (P_∞) vs P which have been shown in **Figure 4.9**. **Figure 4.9a)** shows as soon as the P approaches the critical threshold, the S value undergoes a rapid transition where isolated clusters start merging together to form larger clusters. This sudden emergence of larger clusters leads to the huge gain in the mean cluster size (S) before network formation. On the other hand, P_∞ vs P plot provides a visual representation of how the probability of percolation evolves as a function of the fraction of occupied sites in **Figure 4.9b)**. According to our SEM data this plot typically exhibits a point at which the percolation probability sharply increases from 0 to 1 (Figure 4.4**c)**), indicating sudden variation of the structure.

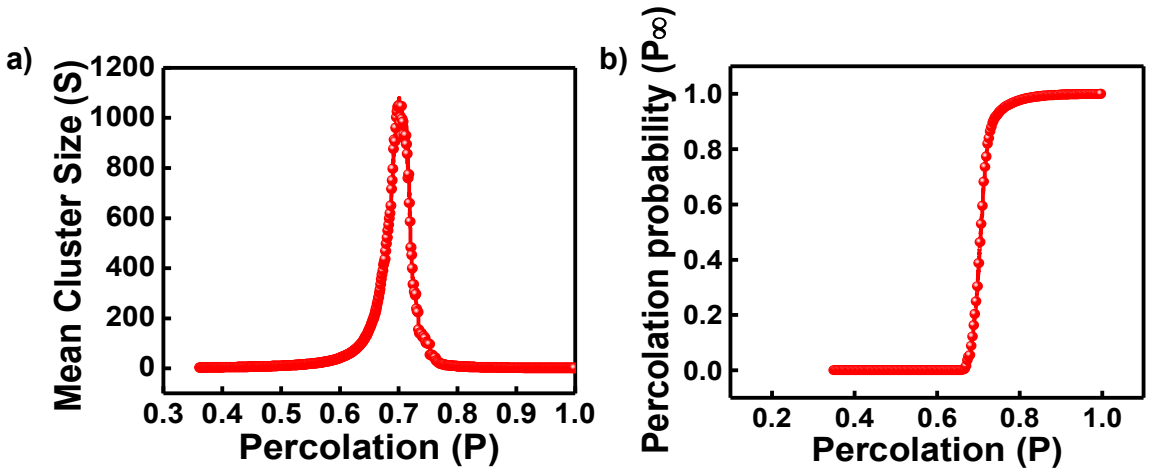

Figure 4.9 Computer-generated Newman-Ziff cluster algorithm data **a)** shows the variation of mean cluster size (S) vs percolation (P) **b)** shows the variation of percolation probability (P_∞) vs Percolation (P). Each point represents the average of 100 distinct arrangements.

TEM analysis of the 10 nm Ag/Ag-TiO_2 TC film is performed for particle size distribution, as illustrated in **Figure 4.10**. For sample preparation, entire film is scratched out with the help of a clean biological surgical blade and collected on a plastic microtube. After the sample is collected, it is dissolved in isopropyl alcohol and dispersed it for 5 minutes in a probed sonicator. Subsequently, a diluted 10 µL drop of this dispersed solution is collected

into a copper coated TEM grid and dried out on a vacuum desiccator for 2 h before characterizing the sample. The Ag NPs have grown within the TiO_2 matrix quite consistently, as seen in **Figure 4.10a)**. From HR-SEM investigation, these results demonstrate that most of the NPs have a size between 5 and 18 nm, with an average particle size of 10.62 nm (**Figure 4.10b)**). Individual lattice d-fringe of Ag NPs and TiO_2 is shown by HR-TEM image (**Figure 4.10c)**) of as prepared sample, suggesting their separate persistence. The average d spacings of Ag NPs and TiO_2 are 0.214, 0.245, and 0.355 nm, respectively, which correspond to the Ag (200), Ag (111), and anatase TiO_2 (101) planes. All these spacings are also defined by the selected-area electron diffraction (SAED) pattern **Figure 4.10d)**, which is well matched with the same set of planes of XRD for 10 nm Ag/Ag-TiO_2 film (Figure 4.1).

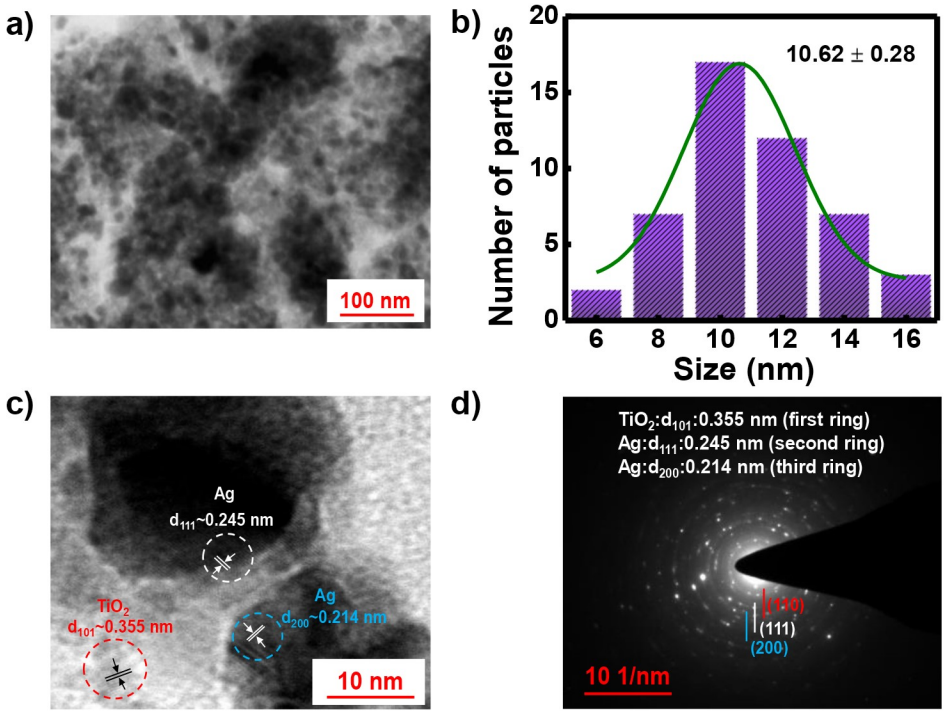

Figure 4.10a) TEM image of 10 nm/Ag-TiO_2 **b)** particle size distribution fitting curve calculated from TEM image **c)** HR-TEM image, the white and bluish ring suggests the lattice d fringe of Ag NPs and reddish ring is of TiO_2 **d)** SAED pattern of 10 nm Ag/Ag-TiO_2 material.

4.3.4 Hydrophilicity test of the 10 nm Ag/Ag-TiO_2/plastic sample

The surface morphology of the fabricated 10 nm Ag/Ag-TiO_2/plastic films are correlated with its macroscopic wettability by measuring equilibrium contact angle (θe) using a host of sessile liquid droplets of constant volume (10 µl), as depicted in **Figure 4.11a)**. The θe of water, ethylene glycol (EG), and N, N-Dimethylformamide (DMF) evolve over time to reach equilibrium values. For a substrate, θe>90° indicates poor wettability and hydrophobicity, while θe<90° indicates good wettability and hydrophilicity. The apparent macroscopic contact angles for different liquid droplets are shown in **Figure 4.11b,c&d)**, with real-time droplet images. The 10 nm Ag/Ag-TiO_2 film on plastic is hydrophilic for all test liquids due to the high surface energy attributed to Ag and TiO_2, which attract polar solvents more strongly. Exposure to UV light during the film development generates hydroxyl groups on the surface, facilitating hydrogen bond formation with polar solvents and resulting in decreased contact angles. Surface roughness also influences wettability; smoother surfaces allow liquids to spread more easily, reducing contact angles. The equilibrium contacts angle for water, EG, and DMF are 58.23°, 42.73°, and 27.34°, respectively. EG and DMF have lower surface tensions than water, leading to easier spreading on the film surface. The surface tension values of the test liquids are sourced from literature, as listed in below (**Table 4.3**).

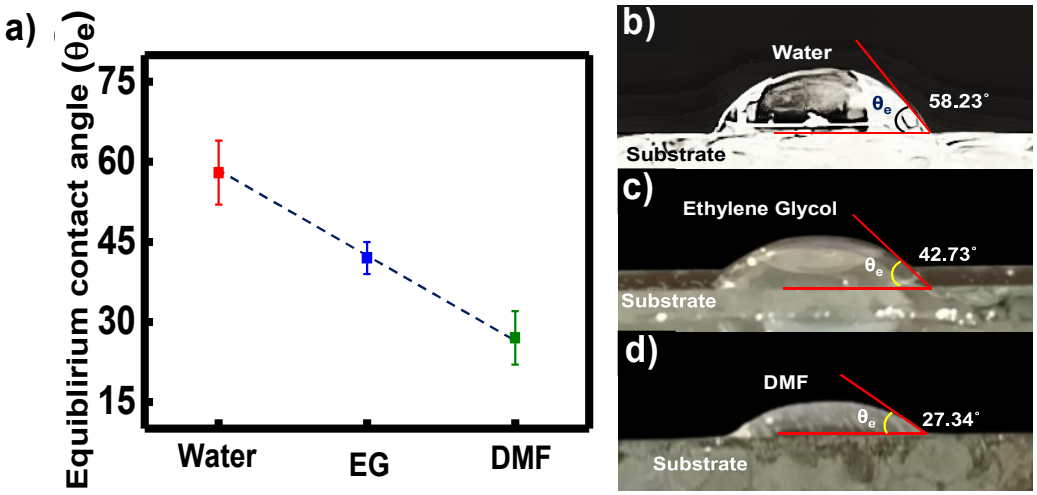

Figure 4.11a) Variation in the equilibrium contact angles, θe with test liquids arranged in decreasing order (L – R) of their liquid–vapour surface tension, γ_l for substrates of specific 10 nm Ag/Ag-TiO_2 film; Real time droplet images on film showing contact angles with **b)** water, **c)** EG, and **d)** DMF respectively.

Table 4.3 Surface Tension Value of Test Liquids

Test Liquid	Water	Ethylene Glycol	DMF
Surface Tension (mN/M)	72	47.7	37.1

4.3.5 UV-Absorption Study

The **Figure 4.12a&b)** shows the picture of comparative transparency of the 10 nm Ag/Ag-TiO_2 sample w.r.t references. Visible transmittance of the conducting film is over 70% where reference (Ag coated plastic) sample shows poor visible transmittance below 60% (**Figure 4.12c)**). Normalized UV-Vis absorption spectra of LTO and 10 nm Ag/Ag-TiO_2 thin films spanning in the 300-900 nm wavelength range are shown in **Figure 4.12d)**. This data indicates the absorption of LTO thin film is in the UV-region (300-350 nm) only whereas the absorption data of 10 nm Ag/Ag-TiO_2 thin film shows an extended absorption in the visible range with an Ag plasmonic peak at 510 nm. The broadening of plasmonic absorption originated due to the large variation of Ag nanostructure of the film morphology.

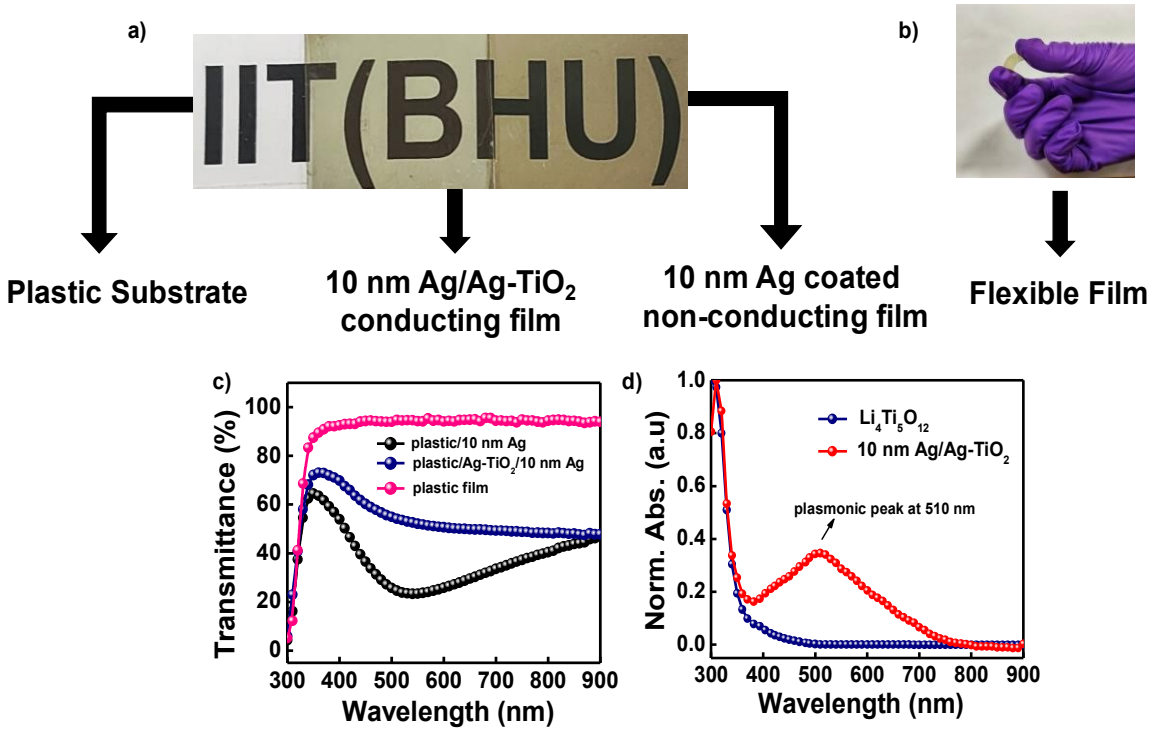

Figure 4.12a) Comparison of optical transparency with plastic substrate, 10 nm Ag/Ag-TiO_2 transparent conducting film and 10 nm Ag coated non-conducting film **b)** image of flexible transparent conducting film **c&d)** optical transparency & UV-Vis absorption spectra of 10 nm Ag/Ag-TiO_2 thin films with reference sample.

4.3.6 Photocurrent Generation under Light

As mentioned earlier, plasmonic photodetectors have been fabricated on top of n^+-Si, where 10 nm Ag/Ag-TiO_2 film works as top electrode with an active area of 0.84×0.84 mm^2 and n^+-Si works as a bottom electrode. Besides, photocurrent of this device is generated from the hot electron generating due to the LSPR of percolated Ag nanostructure. The surface conduction electrons of Ag-NPs that collectively oscillate in response to incident light, leading to enhanced EM fields near the NPs.[55, 81] This enhanced EM field leads to the absorption of incident photons resulting the generation of hot electrons. During electrical characterization of the device, white light of different intensity has been illuminated from the top side of the device that partly transmits and partly absorbed by Ag/Ag-TiO_2 electrode due to the semi-transparent nature and plasmonic absorption of the electrode respectively. **Figure 4.13a)** shows the device configuration where 10 nm Ag/Ag-TiO_2 is used as a transparent electrode. **Figure 4.13b&c)** linear & semi-log plot of electrical current-voltage parameters of this plasmonic photodetector device under dark and light. Linear I−V characterization data ensures the device is a diode in nature. From this semi-log plot, it is clear that the device is rectifier in nature and reverse photocurrent increases with light intensity. When the light intensity is varied from 0 to 400 W/m^2, reversed bias current at 3 V increases from ~8×10^{-6}A to ~2×10^{-3}A, which 265 times w.r.t the dark current. Furthermore, it has been observed that the reverse bias photocurrent variation is nearly linear with the incident light intensity (**Figure 4.13d)**).

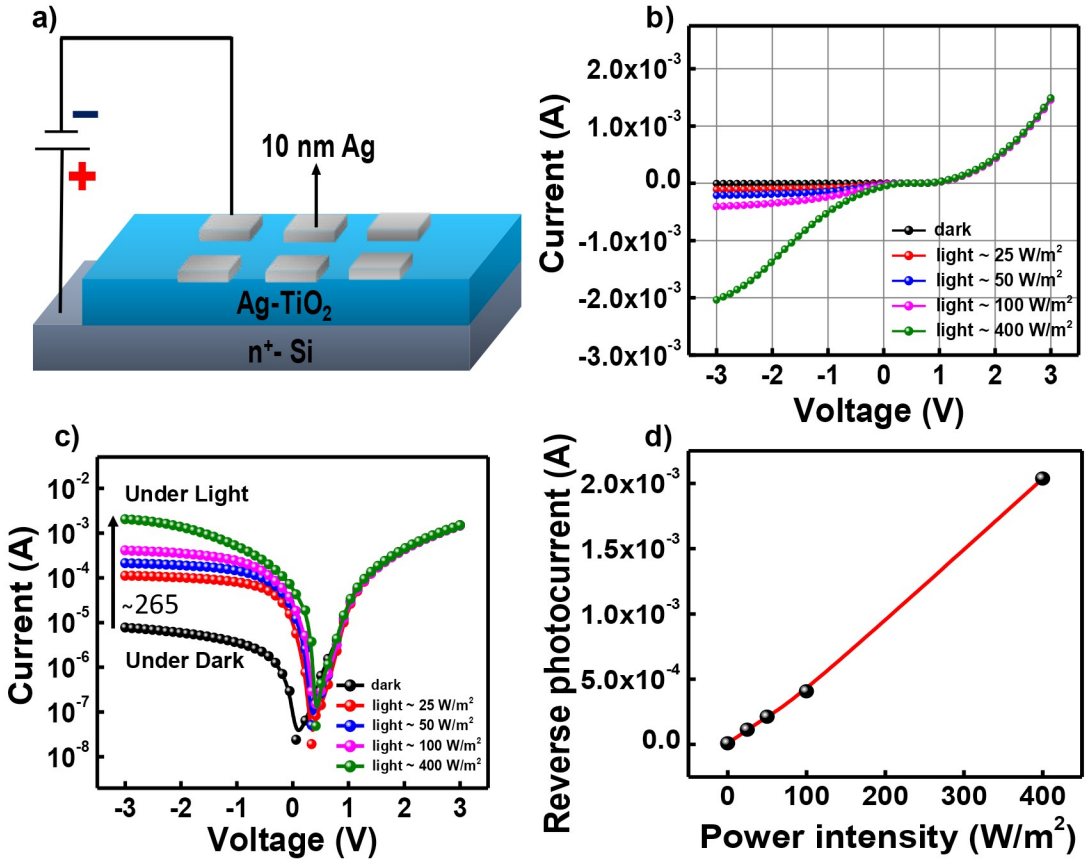

Figure 4.13a) shows device configuration (10 nm Ag/Ag-TiO_2/n^+-Si) **b&c)** linear & semi-log plot which shows immense photocurrent generation of photodiode under dark and light condition **d)** reverse photocurrent vs power intensity curve which shows linear increment of photocurrent generation.

Barrier height and ideality factor of the proposed device under dark and light condition is calculated using **Equation 2.7** and **2.8** respectively. The calculated value of ideality factor and barrier height under dark circumstances are 1.96 and 0.82 eV respectively. Detailed calculation and plots under dark and different light intensities are given in **Figure 4.14a&b)** and **Table 4.4**. Under dark, the ratio of forward bias to reverse bias current at 2 V is ~100. **Figure 4.14c)** shows schematic representations of the relative energy band structure, band bending, and charge separation of the devices under illumination. As soon, light is illuminated, Ag NPs present at top Ag/Ag-TiO_2 electrode exhibit LSPR, leading to strong EM field enhancement near the metal surface, generates hot-electron due to the plasmonic

absorption and subsequently transfers to the conduction band (CB) of TiO_2 and finally reaches to the CB of n^+-Si due to favorable energy band alignment. This rapid charge transfer reduces recombination losses, enhancing the photocurrent generation, thereby improving the photo-response. Hole, on the other hand, is collected by the Ag electrode itself. This generates electron-hole pairs and are separated due to the built-in electric field within the photodiode structure and the different work functions of the electrode materials.

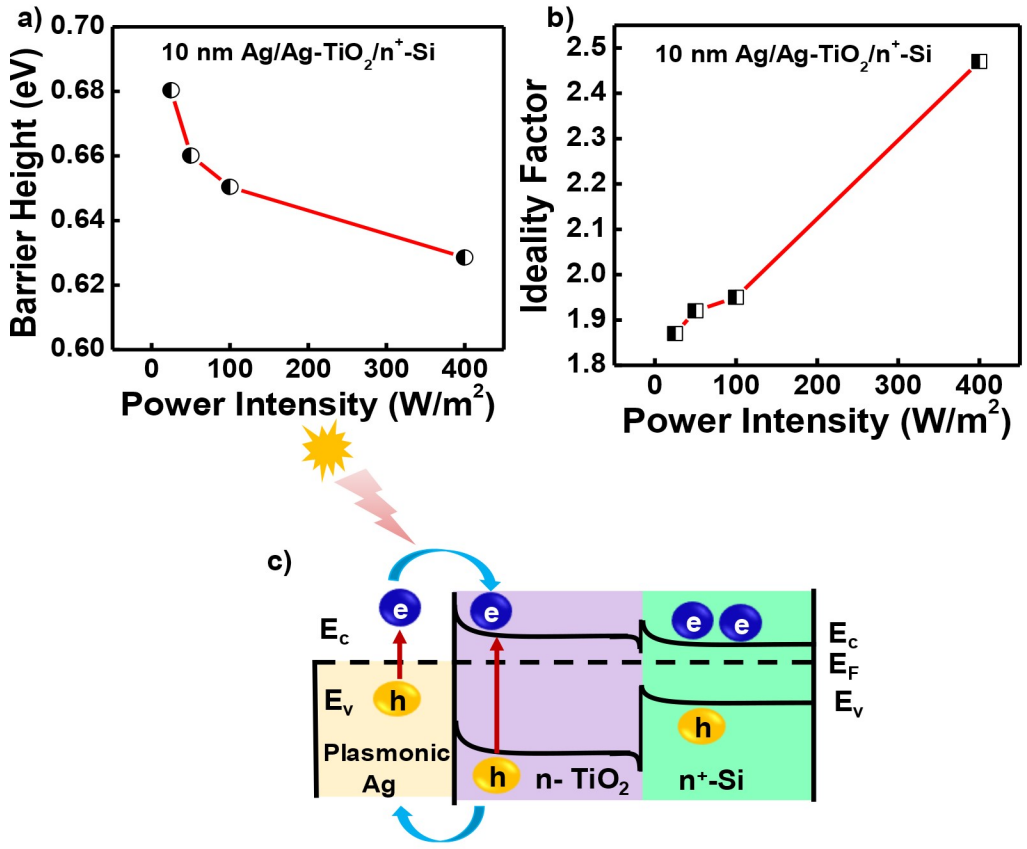

Figure 4.14a) experimental barrier height vs power intensity (Φ_b–P) and **b)** ideality factor vs power intensity (n-P) curve of the 10 nm Ag/Ag-TiO_2/n^+-Si photodiode **c)** band alignment, band bending and charge separation of this hetero-structure photodiode devices.

Table 4.4 Calculated Φ_b and n under dark and different light intensities

Light Intensity (W/m^2)	Barrier Height (Φ_b)	Ideality Factor (n)
0	0.82	1.96
25	0.68	1.87
50	0.66	1.92
100	0.65	1.95
400	0.62	2.47

4.3.7 EQE, Responsivity, Detectivity and Role of Plasmon Induced Hot Electron

The EQE values under different external bias have been measured in the wavelength range of 300 to 1100 nm, as shown in **Figure 4.15a)**. This data implies that EQE value reaches ~ 42.54% at 510 nm under -3V external bias. It can be noted that the EQE spectra of this device is quite similar to the absorption spectra of the Ag/Ag-TiO_2 film (**Figure 4.12d)**) with exactly same peak position (510 nm) which indicates the photocurrent is mostly generated from the plasmon driven hot electron generation. Responsivity and detectivity of the device is calculated from EQE measurement by using **Equation 1.3** and **1.4** respectively. The variation of photo-responsivity under different external biases is depicted in **Figure 4.15b)**. These results show that a maximum responsivity of 15.28 (A/W) can be achieved at 510 nm with an external bias of -3V. As a plasmonic photodetector, this responsivity data is reasonably higher than earlier reports. Besides, detectivity is another fundamental device parameter that suggests the device sensitivity with respect to the minimum signal that can be detected by the photodetector. The variation of the device's detectivities is shown in **Figure 4.15c)**. The highest detectivity of this heterojunction photodetector that has been calculated is of 2.84×10^{12} Jones at 510 nm under -3 V external bias. It is worth mentioning that the plasmonic absorption peak coincides perfectly with the peak of the detectivity at 510 nm, indicating the hot electron of the Ag NPs is primarily responsible for this device's photocurrent generation.

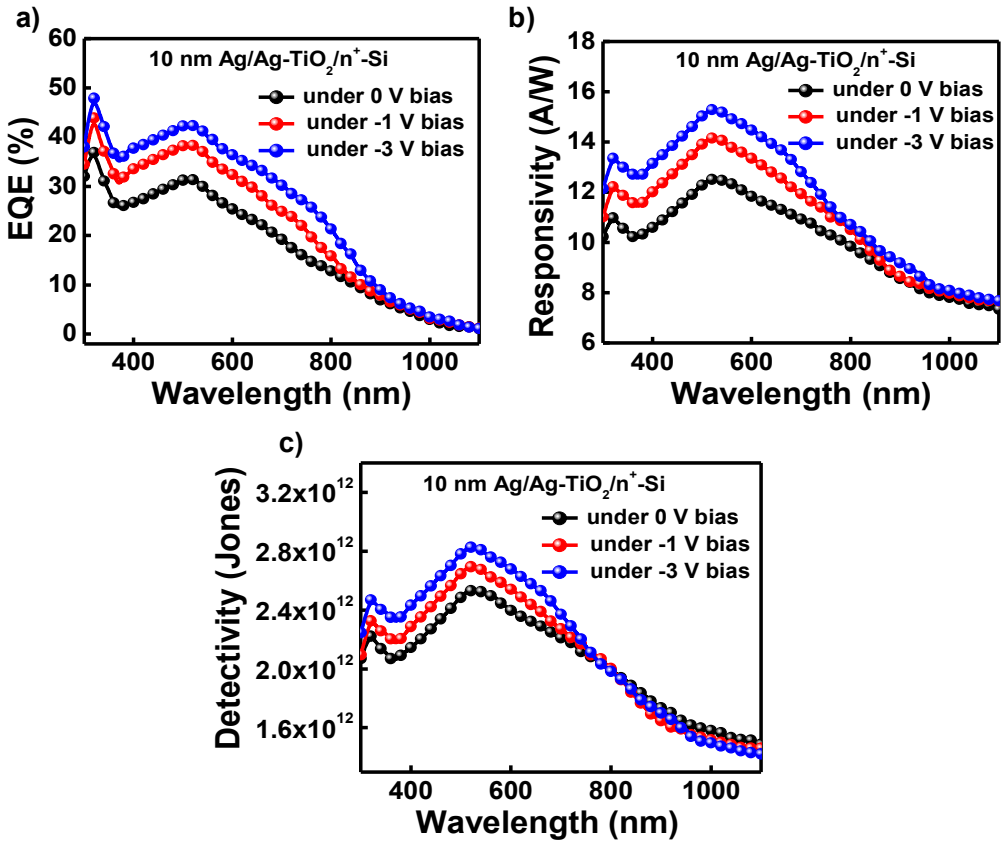

Figure 4.15 illustrates the performance of (10 nm Ag/Ag-TiO_2/n^+-Si) heterostructure photodiode device **a)** EQE vs wavelength **b)** extracted R_λ vs wavelength **c)** extracted D* vs wavelength.

4.3.8 Transient Time Response

Beside device photosensitivity, transient photo response is another key parameter of a photodetector that implies how fast a device can respond and how promptly it can back to its original stage for detecting the next signal. To determine the photo-response of these devices a white light pulse of width and separation of ~ 5 s is illuminated on the device. During this study, the device is subjected to -1V external bias. Photocurrent of the device increases with light intensity, as shown in (**Figure 4.16a)**). Moreover, this transient photocurrent data which is shown in **Figure 4.16b)**, reveals that the device's rise and decay time are ~ 12.36 ms and ~ 12.64 ms respectively, indicating the device has fast photo response and recovery time. Faster transient times are necessary for high-speed applications like optical communication and real-time photography because they indicate a quicker response to changes in light

intensity. A consistent transient response over multiple cycles indicates stable performance, which is important for long-term use in practical applications. Moreover, effective transient response analysis also aids in optimizing the self-bias mechanism to reduce power consumption and boosts energy efficiency of the device. Furthermore, devices are stored in an ambient atmosphere for a few months, although its photosensitivity and transient time remains almost the same, indicating its very high atmospheric stability.

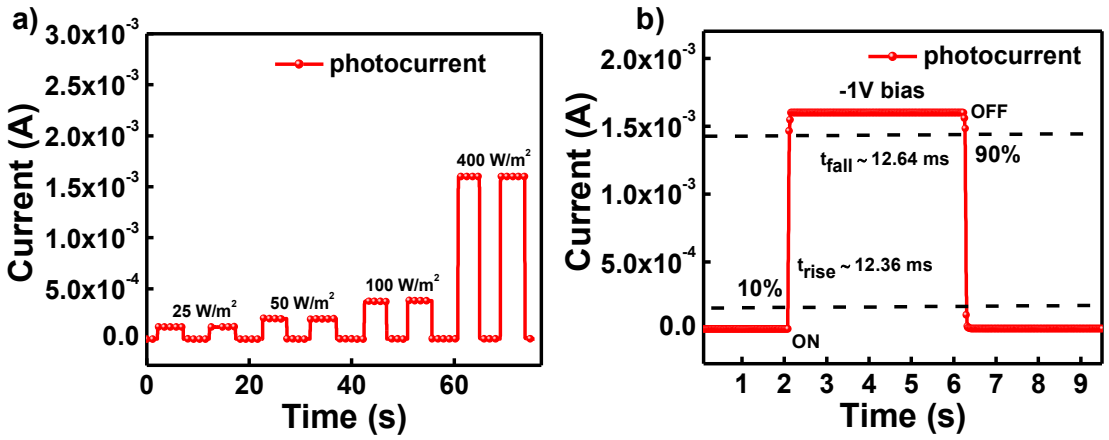

Figure 4.16a) shows the time response of the device **b)** single cycle time response data with rising and decaying times of ~ 12.36 ms and ~ 12.64 ms, respectively.

For a comprehensive assessment of our device's performance, a summary of previously published work on photodetectors based on plasmonic hot electrons is presented in **Table 4.5**. It can be noted that earlier investigations into hot-electron photodetectors have primarily focused on spectral response (R_λ) and the rise-to-fall time ratio (t_{rise}/t_{fall}). Although, important parameters of the hot electron photodetectors are the EQE and D* spectra analysis from where contribution of the hot-electron can be realized, have not been explored in most of the reports. Again, in our previous work on the Ag-TiO_2 based hot-electron photoconductor device (ACS Applied Nano Materials 2023, 6 (16), 15119−15127) photo response is very slow with poor EQE (2.76%) and detectivity (3.19×10^{11}). In comparison to other reported hot-electron photodetectors, this (10 nm Ag/Ag-TiO_2/n^+-Si) plasmonic hot-electron photodetector exhibits a higher responsivity, higher detectivity with extremely fast response speed.

Table 4.5 Comparison of the performance of the current plasmonic hot electrons photodetector with that of other similar devices employing plasmonic hot electrons

Device	λ (nm)	EQE (%)	R (A/W)	D^*(Jones)	τ_r/τ_f	Ref.
10 nm Ag/Ag-TiO_2 / n^+- Si	510	42.54%	15.28	2.82×10^{12}	12.3/12.6 ms	This Work
Ag-TiO_2/TiO_2/ SnO_2/glass	420	2.76%	0.98	3.19×10^{11}	1.2/0.95 s	[106]
Porous Ag/TiO_2/Ti	450	–	3.3×10^{-3}	9.8×10^{10}	112/24 μs	[165]
Ag/TiO_2 NTs/FTO	370	–	176.30	–	82/14 s	[172]
Porous Au/Si	–	–	3.5×10^{-3}	–	–	[173]
Au nanorods/Si	–	–	1.0×10^{-5}	–	–	[154]
Au/Pyramid-Si	1200	–	8.2×10^{-3}	1.8×10^{10}	–	[159]

4.4 Conclusions

In conclusion, a sol-gel derived synthesis technique has been developed to deposit LTO thin film on mechanically flexible plastic substrate at low temperature by combined heating (at 100˚C) and UV illumination. Then, the loosely bound Li^+ of this thin film has been replaced by Ag^+ through an ion-exchange process that forms an Ag-TiO_2 thin film. A thermally evaporated 10 nm Ag has been deposited on top of this Ag-TiO_2 thin film, which shows high electrical conductivity (50 ohm/□) and over a 70% average visible transmittance in the range

of 350-450 nm wavelength. This high electrical conductivity of the film appears due to the higher lateral growth of Ag during thermal evaporation w.r.t reference clean plastic substrate. A growth mechanism has been proposed to understand this Ag NPs induced lateral growth of the film. This film also shows a vibrant plasmonic absorption that limits the transparency of the film. By utilizing combined optical transparency and plasmonic absorption features of this thin film, a plasmonic photodetector has been fabricated on top of a n^+-Si substrate where, 10 nm Ag/Ag-TiO_2 thin film works as plasmonic electrode and n^+-Si substrate as counter electrode. Device shows a very high photosensitivity in the visible region. It has been observed that the EQE spectra of this device has a great similarity with the absorption spectra of 10 nm Ag/Ag-TiO_2 thin film. Same absorption and EQE peak position (510 nm) reveals that the contribution of plasmonic hot electron is highly responsible for the photocurrent generation of the device. Device shows very high EQE, photo responsivity, and detectivity of values 42.54%, 15.28 A/W, and 2.84×10^{12} Jones, respectively at (510 nm). Moreover, devices show extremely fast photo response with a rise and decay times of 12.36 ms and 12.64 ms respectively. Overall performance of this plasmonic photodetector is significantly higher than the previously reported article, that gives a visible way to fabricate reliable hot electron-based photodetectors.

Chapter 4

2nd Part: Cost Efficient Ag/Ag-TiO_2 Coating Based Flexible Transparent Heat Reflector for Energy-Saving Smart Window

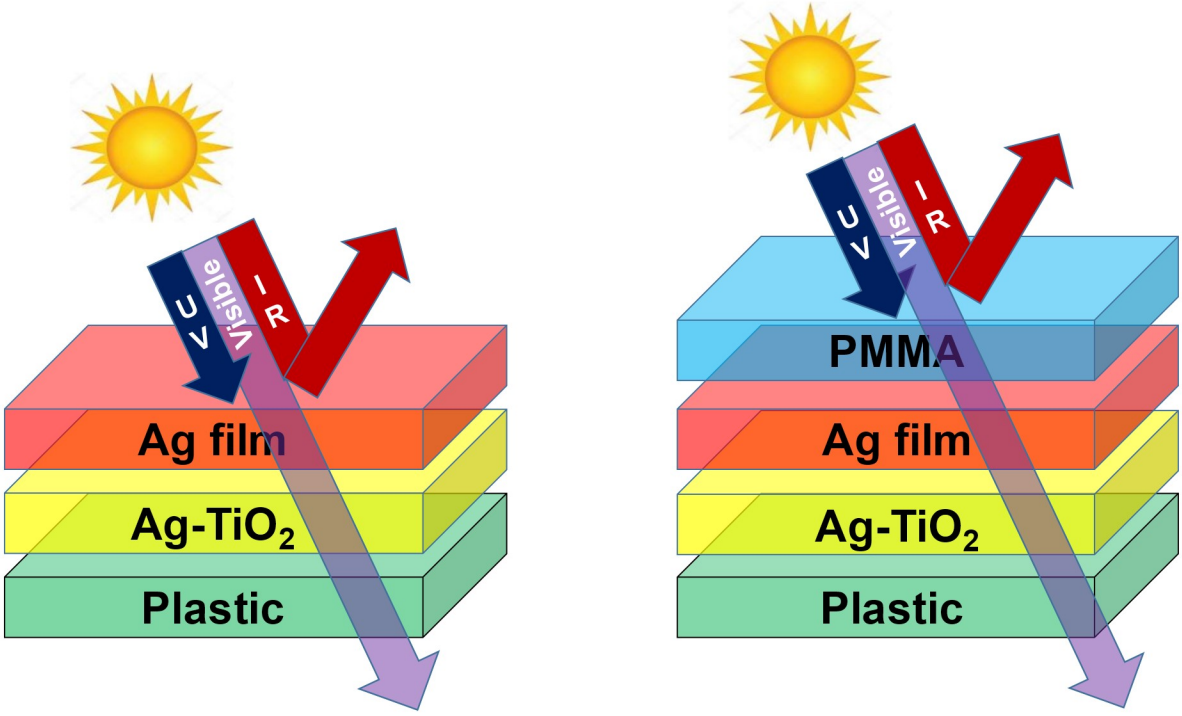

This work is a continuation of chapter 4 first part for the development of a mass-producible and low-cost transparent heat reflector (THR) on a flexible PET substrate by using a per-deposited Ag nanostructures thin film which is grown in two step deposition method. Initially, a polycrystalline LTO thin film has been grown on a plastic substrate by a low temperature processed sol-gel technique. Afterword, mobile Li^+ of LTO thin film has been replaced by Ag^+ by an ion-exchange method to form Ag-TiO_2 thin film. In the second step, 10 nm Ag has been deposited on top of Ag-TiO_2 thin film by thermal evaporation. This bilayer THR has IR/NIR reflectivity of ~85-90% in combination with its visible transmittance of ~50-70%. For higher environmental stability of this THR, a polymer film (PMMA) has been coated on top of this Ag/Ag-TiO_2 coating. To realize the practical application of this THR, a prototype box with one transparent glass window coated with this THR film has been developed and its internal temperature has been investigated during daytime. A reduction of internal temperature of ~6-7˚C has been observed due to this THR coating w.r.t the reference uncoated box, indicating its plausibility as energy-saving smart window applications.

4.5 Introduction

The major source of contemporary global warming and environmental degradation is the utilization of fossil fuels.[204-206] One way to significantly reduce worldwide energy usage is to develop and implement an efficient cooling or heating system that maintains interior comfort using minimal electricity.[207, 208] The design of next-generation smart windows holds a long-term influence on the environment's sustainability,[209] energy consumption efficiency[210, 211] and human health behavior. THR coating has a high reflectivity in NIR/IR radiation with high transmittance in the visible region.[212-215] Heat flux mainly quantifies the amount of thermal energy transferred per unit time through a unit area. Heat flux through a material, particularly in the context of windows, depends significantly on the position of the visible (380-760 nm) to NIR/IR (700-2500 nm) bands. It is known that the heat flux from visible light is significantly lower compared to NIR. In earlier work, it has been demonstrated that approximately ~50-60% of heat flux of solar irradiation exists in the

NIR region compared to the visible region (~10-15%).[216, 217] Therefore, it's very important to develop a NIR/IR reflecting coatings to a window for blocking heat transmission through the glass during daytime, saving energy for air conditioning cooling cost throughout the summer.[218, 219] Simultaneously, sufficient transmission efficiency in the visible spectrum of the window is required to ensure optimum visibility which can reduce the daytime electric cost of light. Traditional glass windows not only enable the visible light to pass through it, but also allow heat transmission through it, which in turn increases the indoor temperature. Therefore, THR materials must be highly transparent in the visible region (350-650 nm) and should have a high NIR/IR reflectivity (700-5000 nm).[125, 126, 220, 221]

Till now a number of concepts have been introduced to develop high performance THR. Among them sandwiching a thin layer of metal in between two dielectrics in a dielectric/metal/dielectric (DMD) is the most successful approach.[222, 223] However, the fabrication cost of these multilayer stacked structures is not economical in most of the cases. These DMD structure are mostly developed based on different physical vapor deposition like sputtering, e-beam evaporation and also frequently include expensive materials like Au for its optimum reflectivity spectra in NIR/IR region, but its potential is limited by its steep cost.[224] Besides, thermo-chromic materials[225-229] have also been widely studied because of their temperature dependent transmission/reflection properties. Although the performance of such thermo-chromic materials as THR depends on their phase transition temperature.[230] Among different thermo-chromic materials, doped vanadium dioxide (VO_2)[231-236] is widely investigated due to their insulator-to-metal transition that changes the transmission/reflection spectra of this material. It has been observed that foreign cations like W^{6+}, Nb^{5+}, Ti^{4+}, can greatly reduce the transition temperature and make it a promising material for practical application.[237-240] Though, fine tuning of color change in such thermo-chromic materials is a difficult task. On the other hand, Ag has a high IR reflectivity and lower market price compared to Au, is much desirable for the low-cost transparent heat reflecting window application.[241-243]

In this section of this chapter, a low cost and mass-producible fabrication method of Ag-nanostructured based THR has been reported. A percolated Ag film has been grown during thermally deposited Ag film on an Ag-TiO_2 thin film with a critical mass-thickness of 10

nm. This Ag-TiO_2 film is an Ag nanoparticle embedded TiO_2 thin film that has been deposited on a plastic substrate by a solution processed technique in two individual steps. During thermally grown Ag film on Ag-TiO_2 coated substrate, at a critical mass-thickness of 10 nm, Ag nanostructure becomes percolated. This 10 nm Ag/Ag-TiO_2/plastic shows a visible transmittance of around ~50-70% with an average ~85% reflection in the NIR/IR region. To realize its practical application as THR, a prototype box with one transparent wall coated with this Ag/Ag-TiO_2 film has been developed and its internal temperature has been investigated during daytime. A reduction of internal temperature of ~6-7˚C has been observed due to this coating w.r.t the reference uncoated box.

4.6 Experimental Section

4.6.1 Preparation of Precursor Materials

The synthesis process for LTO via low temperature solution process technique has been explained in **Chapter 2 Chapter 2 Section 2.1.1.** PMMA is used as a protective coating for THR film. The solution is prepared by standard method, reported in **Chapter 2 Section 2.1.7**.

4.6.2 Fabrication of THR Film

The Ag/Ag-TiO_2 based THR film has been fabricated on a flexible PET substrate and the fabrication steps has been explained **Chapter 2 Section 2.3.2**, and schematically present in **Figure 2.7**.

4.7 Results and Discussion

4.7.1 Structural Evaluation (XRD analysis)

Step-by-step XRD analysis of THR film is similar with previous work and discussed earlier in **Chapter 4 Section 4.3.1**.

4.7.2 Surface Analysis (HR-SEM, AFM & HR-TEM)

Surface morphology of Ag/Ag-TiO_2 thin film of different Ag thickness is studied by HR-SEM and AFM. HR-TEM study is done to understand the average particle size of Ag NPs formation within the THR film. Detail study of morphological changes is explained in **Chapter 4 Section 4.3.3**.

4.7.3 Optical Study (Reflectance & Transmittance Spectra)

The optical transmittance and reflectance of Ag/Ag-TiO_2 film for different thickness of Ag film ranging from 10 nm to 14 nm is presented in the **Figure 4.17a&d)** with a fixed thickness of Ag-TiO_2 film. From the reflectance spectra, it can be observed that the reflectance of all these films has reached around ~ 85 % in the range above 1000 nm long with a transparency ~ 70 % in the blue region and ~ 50-60 % in the rest of the visible region. It is also noticed that the increasing thickness of Ag from 10 nm to 14 nm makes it more IR/NIR reflecting while visible transmittance decreases simultaneously. In the visible wavelengths, the transmittance spectra are influenced by absorption of light in the Ag thin film due to plasmonic absorption, which is associated with the interband electronic transitions, due to the excitation of electrons from the d-band to the fermi surface. By increasing the thickness of the Ag layer, larger number bound electrons are excited and therefore transmission reduces further. However, the surface coverage by Ag film increases a bit that results in a small enhancement of reflectance, both in UV-Vis and NIR region. Furthermore, reflectance spectra have been measured up to 5000 nm by a FTIR spectrophotometer. This study indicates the reflection spectra is very flat in the higher wavelength range and reached around 90% as shown in **Figure 4.17b)**. Similar reflectance and transmission studies have been performed with protective PMMA coated Ag/Ag-TiO_2 film with different thickness of Ag layer ranging from 10 nm to 14 nm which is shown in **Figure 4.17c&e)**. In this work PMMA coating has been utilized for the long-term environmental stability of the Ag/Ag-TiO_2 coating. It has been observed that an uncoated Ag/Ag-TiO_2 film starts oxidizing after 3-4 days and affects its optical properties like transmission & reflectance. High visible transmittance and IR/NIR reflectance are the key factors for designing a transparent heat reflector. For this clarification, a graphical presentation has been provided in **Figure 4.17f)**, which shows the transmittance at λ=375 nm and reflectance at λ=1800 nm with different thickness of Ag film. As shown in this figure, transmittance of these Ag/Ag-TiO_2 films

remain within ~ 65-70 % whereas reflectance remains ~ 85-90 %. Moreover, with increasing thickness of Ag, transmission decreases and reflectance increases.

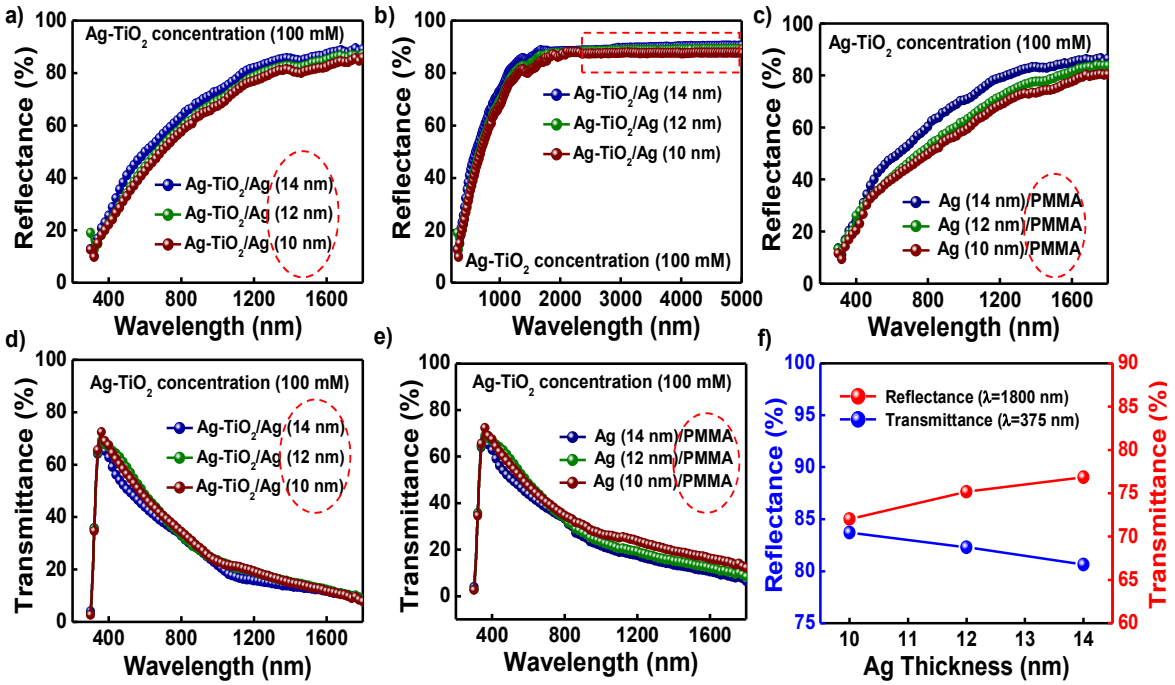

Figure 4.17a) Reflectance spectra of Ag/Ag-TiO_2 film with different thickness of Ag layer ranging from 10 nm to 14 nm **b)** extended reflectance spectra of the film upto far infrared region (5000 nm) **c)** reflectance spectra of the film with PMMA as a protecting layer **d&e)** transmittance spectra of THR film without and with protecting layer **f)** varience of reflectance (λ= 1800 nm) and transmittance (λ=375 nm) spectra ranging from 10 nm to 14 nm thickness of Ag film with fixed Ag-TiO_2 film thickness.

For comparative study with and without coated PMMA over the film as a top matrix, shows optical reflectance and transparency data over the time span of 7 days for a particular wavelength, which is shown in (**Figure 4.18a&b**). However, such oxidation (or color change) is not observed in a 6-month-old PMMA coated Ag/Ag-TiO_2 THR film. Besides, this film is more stable under mechanical bending and also protects the Ag/Ag-TiO_2 coating from mechanical scratching.

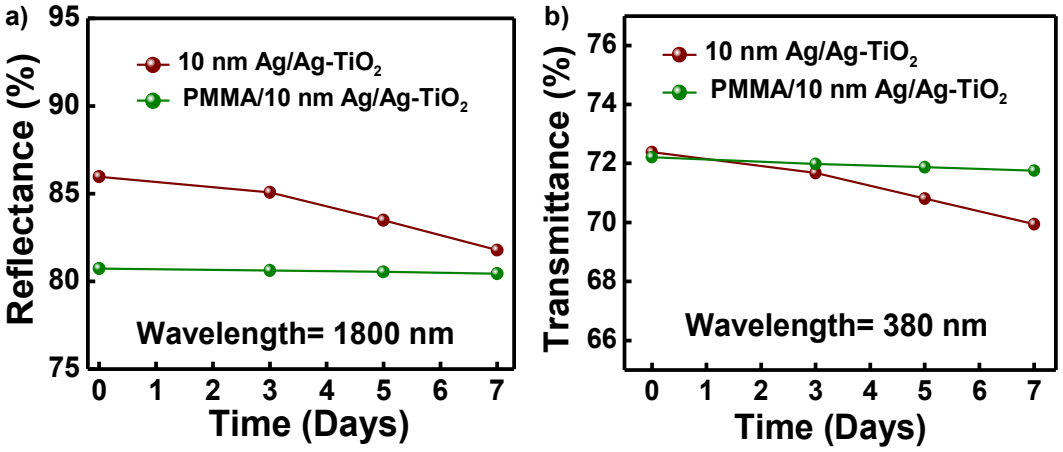

Figure 4.18a&b) Stability comparision of reflectance (at R = 1800 nm) and transmittance (at T= 380 nm) data of 10 nm Ag/Ag-TiO_2 coated THR film with and without PMMA matrix.

To optimize the optical properties of THR, a detailed investigation has been performed by varying the thickness of Ag-TiO_2 layer. From this study, it has been identified that the optimized Ag-TiO_2 layer can be obtained from the LTO precursor concentration of ~100 mM. The cross-sectional SEM study of this Ag-TiO_2 thin film (LTO concentration ~ 100 mM) indicates its thickness of ~ 20 nm (**Figure 4.6c)**). The variation of reflectance and transmittance spectra with different thickness of Ag-TiO_2 layer and fixed thickness of Ag film (10,12&14 nm) is shown in **Figure 4.19a,b,c,d,e&f)**.

To identify the role of Ag-TiO_2 film for THR fabrication, a comparative reflectance and transmission data of 10 nm Ag thin film grown on bare plastic and Ag-TiO_2 coated plastic film are provided in **Figure 4.20a&b)** respectively. In this presentation, reflectance and transmission data of bare plastic film is also provided as reference. This data clearly shows 10 nm Ag film that grown on a bare plastic film has a very poor reflectance in NIR/IR region (~20%) w.r.t the Ag/Ag-TiO_2 layer (~80-85%), whereas the reflectance of bare plastic is only ~16% throughout the spectra. Similarly, comparative transmission data shows that the 10 nm Ag film that grows on Ag-TiO_2 layer has a very poor transmission in the IR/NIR region (~30% at 800 nm)) and its gradually decreasing with wavelength (~20% at 1800 nm).

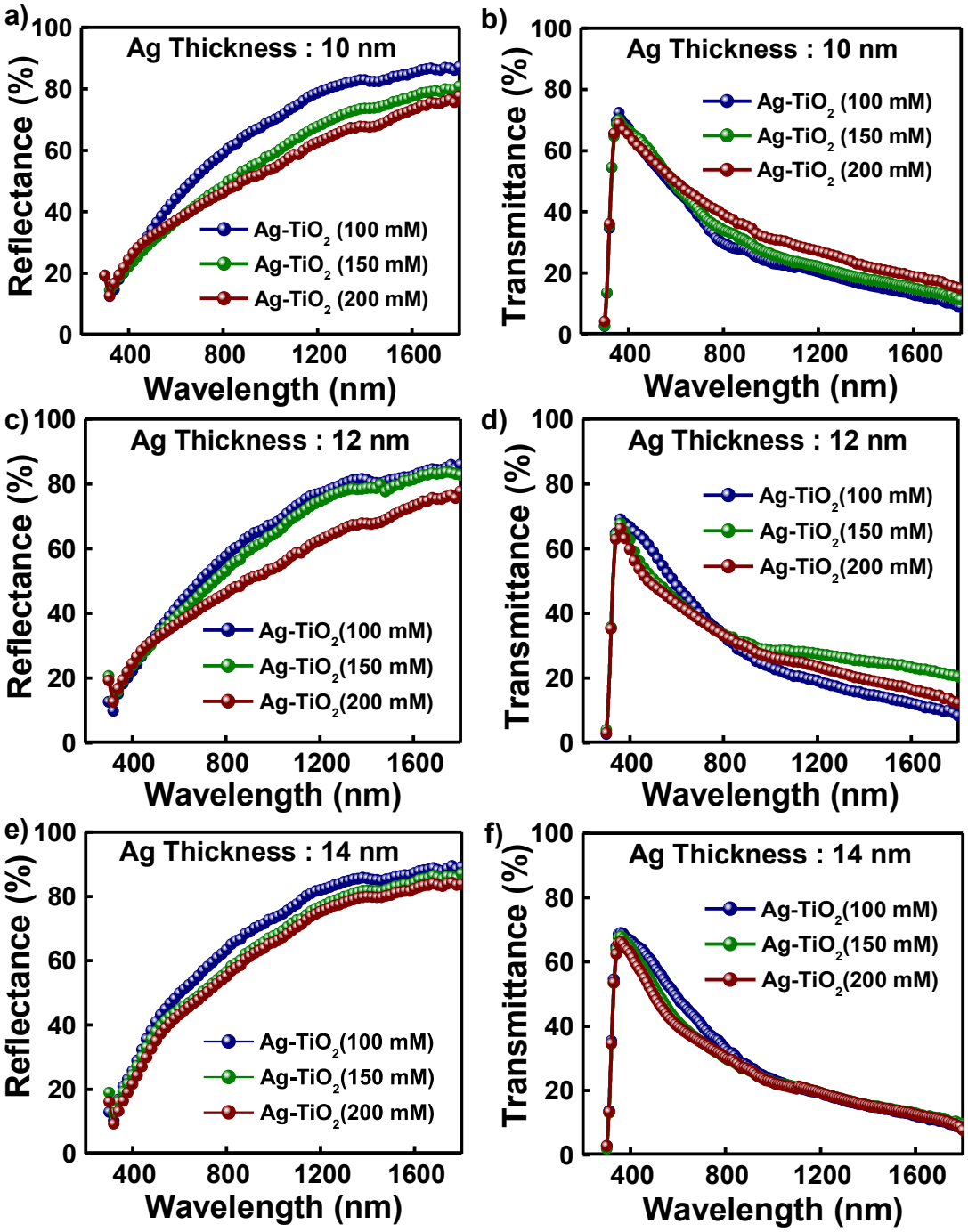

Figure 4.19a,b,c,d,e&f) Reflectance & transmittance spectra of 10,12&14 nm Ag/Ag-TiO_2 THR film with different thickness of Ag-TiO_2 layers varying approximately from 20 nm to 40 nm.

In contrast to that, the 10 nm Ag film on bare plastic shows very high transmission in the NIR/IR region with a dip in the visible region. That dip originated from the strong plasmonic absorption from the granular Ag film that grows on bare plastic, shows that the transmission of the bare plastic substrate is ~ 90% throughout the spectra. The reflectance and transmission data of relatively lower thickness Ag/Ag-TiO_2 film have presented in **Figure 4.20c&d)** respectively. From Figure 4.20**c)** it's very clear that the reflectance of 6 and 8 nm Ag film is very poor (~20%) throughout the spectra whereas reflectance of 10 nm Ag film is very high (~70-85%) in NIR/IR region which is totally different from lower thickness Ag films. The transmission data of these films shows that 6 nm Ag film in NIR/IR region is very high (~60-80%), while 8 nm Ag film has relatively lower transmittance (~40% in NIR/IR region). On the other hand, the transmission of 10 nm Ag film in NIR/IR region is very poor which is due to their high reflecting properties.

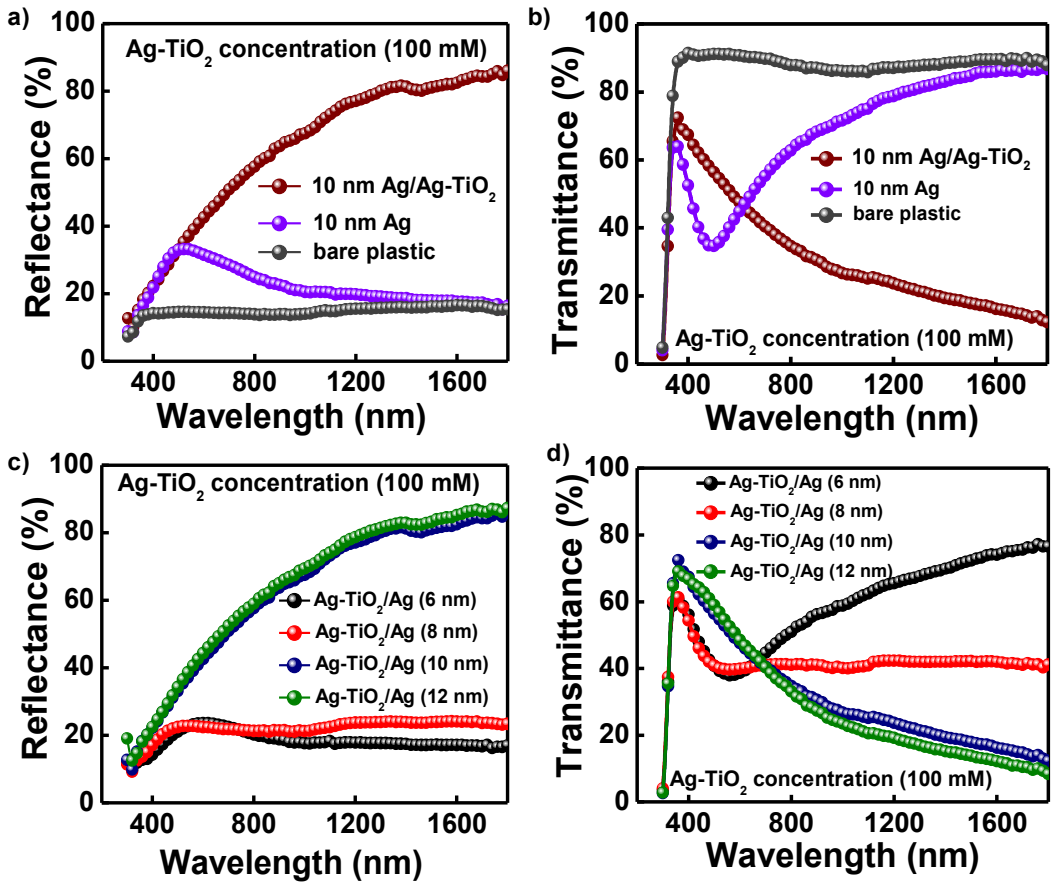

Figure 4.20a&b) Comparison of optical reflectance and transmittance of bare plastic, 10 nm Ag film on bare plastic and 10 nm Ag/Ag-TiO_2 bilayer THR thin film; **c&d)** reflectance &

transmittance data of different thermal evaporated Ag film ranging from 6 nm to 12 nm in present of Ag-TiO_2 thin film.

Figure 4.21a) demonstrates the variation of visual observation of different thickness of Ag/Ag-TiO_2 film. It's clearly shown from the picture that the transparency of 14 nm Ag/Ag-TiO_2 film is significantly lower compared to 10 nm Ag/Ag-TiO_2 film thickness. **Figure 4.21b)** shows the transparency and reflectance of 10 nm Ag/Ag-TiO_2 transparent heat reflecting coating. **Figure 4.21c)** shows the real image of 10 nm Ag/Ag-TiO_2 film with a background of bright color flowers.

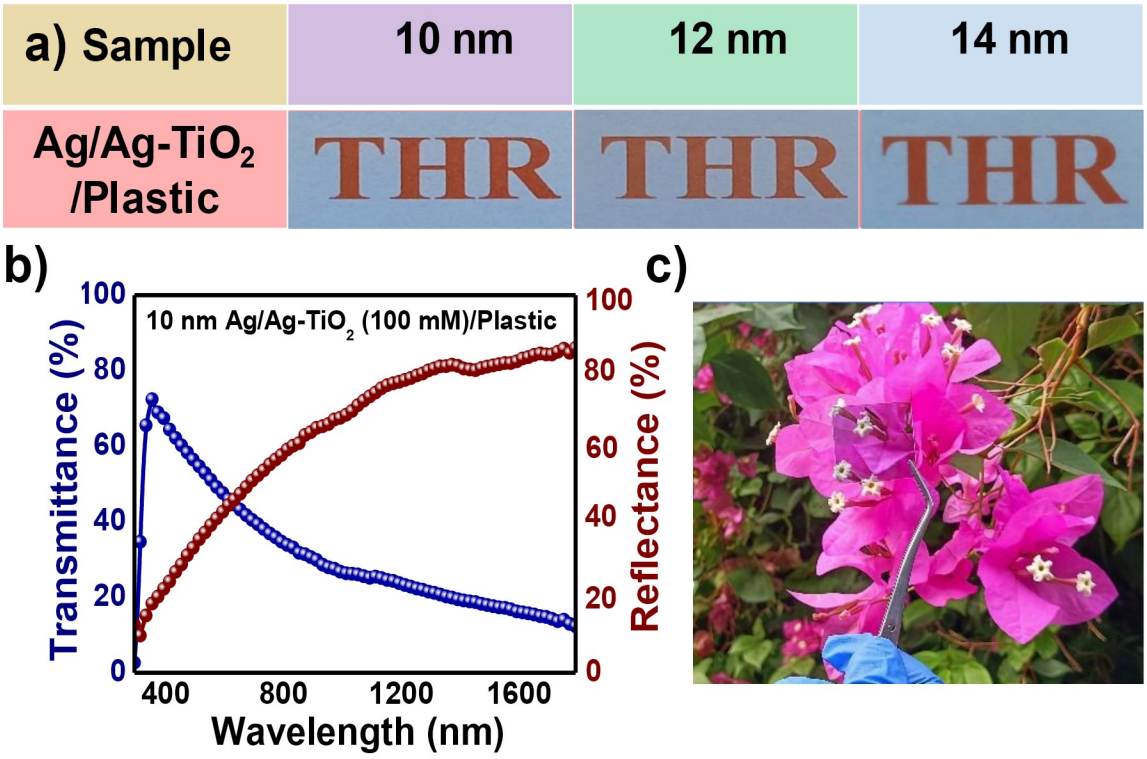

Figure 4.21a) The images of Ag/Ag-TiO_2 transparent heat reflector on plastic substrate at different thickness of Ag film vary from 10 nm to 14 nm with an underlying 'THR' written on a white paper **b)** optical transparency and reflection of 10 nm Ag/Ag-TiO_2 on plastic **c)** practical transparency test with a background of a bight colour flower.

The effectiveness of this 10 nm Ag/Ag-TiO_2 coating as a transparent heat reflector has been investigated throughout a daytime temperature monitoring with a prototype box that has one transparent wall coated with this THR (real photo is attached in **Figure 4.22**. Two identical

thermocol covered wall boxes of dimension 15×15×15 cm^3 with a glass window wall of (10×10 cm^2) have been prepared. In one box, the glass window is coated with 10 nm Ag/Ag-TiO_2 whereas reference box glass window is uncoated. These boxes are kept on a rooftop. Then two identical thermocouples are placed inside the closed boxes for monitoring the inside live temperature. Another thermocouple is attached outside the box to check the live air temperature all over the day. Inner walls of these boxes are coated with white, gray and black papers for three sets of individual experiments. The idea of using different colored inner walls for the experiment of daytime cooling performance is to visualize the effect of temperature difference under different color window wall.

Figure 4.22 Experimental set-up under sunlight outdoor experiment.

The variation of temperature inside the 10 nm Ag/Ag-TiO_2 coating box, reference box and outside air temperature have been monitored throughout the daytime and has been given in **Figure 4.23a,b&c).** The average temperature differences of these three different thermocouples in peak hour of the day (from 12 pm to 1 pm), which is shown in **Figure 4.23d)** for different inner walls. With black insulating inner wall ~15˚C temperature differences have been observed between THR coated and uncoated glass boxes while with white wall this difference becomes ~ 3.5˚C. With the gray wall, there is a temperature difference of ~ 7˚C. Since the boxes are closed, heat is accumulating inside the boxes over the time, which increase the inner temperature. Therefore, the temperature of these boxes is significantly higher than open air temperature.

Besides, heat reflecting property of the 10 nm Ag/Ag-TiO_2 coated window with respect to the glass window has been investigated under steady NIR/IR light (IR lamp) illumination. For this study, one digital thermometer and IR lamp is kept 4 cm behind and 6 cm away from the coated window, respectively. Temperature variations of digital thermometers have been monitored over the time. Same experiment has been also performed for reference uncoated glass window. It is observed that the temperature behind the coated window shows an average ~10-12˚C lower temperature compared to the reference glass window, which is shown in the bar diagram (**Figure 4.23e)**). Real picture of the experiment under the IR lamp is shown in **Figure 4.23f)**.

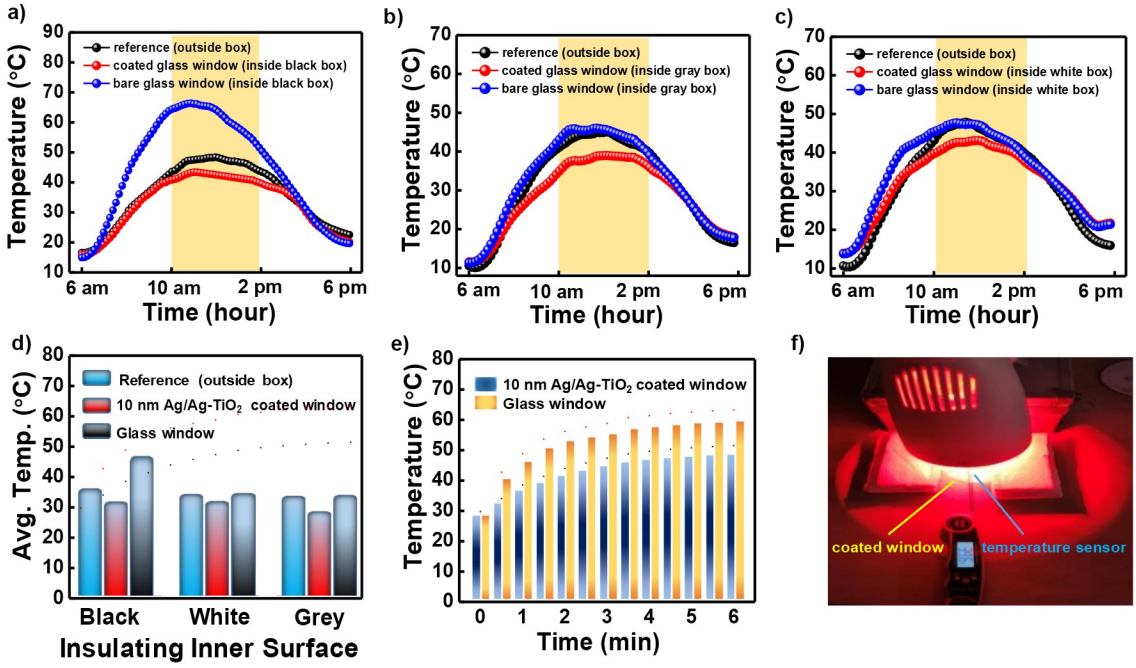

Figure 4.23 Performance of daytime (under sunlight) cooling study of 10 nm Ag/Ag-TiO_2 coated window compare with reference glass window box with inner wall color of **a)** black, **b)** white and **c)** gray; **d)** comparative average temperature difference at the peak hour (12 pm to 1 pm) for different inner color wall of the box; **e)** experimental study (IR lamp) of 10 nm Ag/Ag-TiO_2 coated window compare with glass window; **f)** real image of IR lamp experimental setup

Table 4.6 Comparison of the performance of our develope transparent heat reflector with other material based heat reflecting coating

THR coating	Transmittance at Visible Region	Reflectance at NIR Region	Average Temp. differ. with normal window	Ref.
10 nm Ag/Ag-TiO_2	68-72%	85-90%	6-7ºC	This work
TiO_2/Cu/TiO_2	90%	85-90%	-	[220]
ZnO/Au/ZnO	68-70%	45-50%	-	[125]
TiO_2/VO_2/TiO_2	60-65%	50-55%	-	[126]

4.8 Conclusion

In summary, Ag-based low temperature processed (100˚C) THR has been fabricated on plastic PET substrate. For this deposition, initially Ag-TiO_2 thin film is deposited by a solution processed technique where Ag nanoparticles are grown inside TiO_2 matrix. Subsequently a thermally deposited Ag film is deposited on top of the Ag-TiO_2 thin film. A protective PMMA layer is deposited on top of Ag/Ag-TiO_2 to improve its stability. It is observed that a critical thickness of the 10 nm Ag layer is essential for optimized NIR/IR reflection (~85%) in combination with reasonably high visible light transmittance (~70 % in blue region and ~50-60 % in rest of the visible region). A comparative surface morphology of the Ag/Ag-TiO_2 reveals a morphological phase transition occurs when thermally deposited Ag film reaches 10 nm. During this transition, the circular shape isolated Ag island on Ag-TiO_2 thin film transfers to a percolated finger-like network that has significantly lower roughness than previous stage isolated Ag island film. This phase transition becomes possible due to the lateral growth of Ag induced by pre-existed Ag NPs on TiO_2 matrix. As a consequence, visible transparency of the film increases with an excellent NIR/IR reflectivity. A prototype box with a window coated with Ag/Ag-TiO_2 thin film reveals that a reduction of ~6-7˚C of internal temperature of the box compared to reference glass window, due to the efficient NIR/IR reflectivity of Ag/Ag-TiO_2 thin film. Overall, our approach opens new opportunities to develop highly transparent heat reflecting coating through a low-cost fabrication method which can be utilized for energy saving smart window applications.